

Are Brightest Halo Galaxies Central Galaxies?

Ramin A. Skibba^{1,2*}, Frank C. van den Bosch³, Xiaohu Yang⁴, Surhud More^{1,5}, Houjun Mo⁶, Fabio Fontanot^{1,7}

¹*Max-Planck-Institute for Astronomy, Königstuhl 17, D-69117 Heidelberg, Germany*

²*Steward Observatory, University of Arizona, 933 N. Cherry Avenue, Tucson, AZ 85721, USA*

³*Department of Physics and Astronomy, University of Utah, 115 South 1400 East, Salt Lake City, UT 84112-0830, USA*

⁴*Key Laboratory for Research in Galaxies and Cosmology, Shanghai Astronomical Observatory; the Partner Group of MPA; Nandan Road 80, Shanghai 200030, China*

⁵*Kavli Institute for Cosmological Physics, The University of Chicago, 5640 S. Ellis Avenue, Chicago, IL 60637, USA*

⁶*Department of Astronomy, University of Massachusetts, Amherst MA 01003-9305, USA*

⁷*INAF - Osservatorio Astronomico di Trieste, Trieste, Italy*

ABSTRACT

It is generally assumed that the central galaxy in a dark matter halo, that is, the galaxy with the lowest specific potential energy, is also the brightest halo galaxy (BHG), and that it resides at rest at the centre of the dark matter potential well. This central galaxy paradigm (CGP) is an essential assumption made in various fields of astronomical research. In this paper we test the validity of the CGP using a large galaxy group catalogue constructed from the Sloan Digital Sky Survey. For each group we compute two statistics, \mathcal{R} and \mathcal{S} , which quantify the offsets of the line-of-sight velocities and projected positions of brightest group galaxies relative to the other group members. By comparing the cumulative distributions of $|\mathcal{R}|$ and $|\mathcal{S}|$ to those obtained from detailed mock group catalogues, we rule out the null-hypothesis that the CGP is correct. Rather, the data indicate that in a non-zero fraction $f_{\text{BNC}}(M)$ of all haloes of mass M the BHG is not the central galaxy, but instead, a satellite galaxy. In particular, we find that f_{BNC} increases from ~ 0.25 in low mass haloes ($10^{12} h^{-1} M_{\odot} \leq M \lesssim 2 \times 10^{13} h^{-1} M_{\odot}$) to ~ 0.4 in massive haloes ($M \gtrsim 5 \times 10^{13} h^{-1} M_{\odot}$). We show that these values of f_{BNC} are uncomfortably high compared to predictions from halo occupation statistics and from semi-analytical models of galaxy formation. We end by discussing various implications of a non-zero $f_{\text{BNC}}(M)$, with an emphasis on the halo masses inferred from satellite kinematics.

Key words: methods: statistical – galaxies: halos – galaxies: kinematics and dynamics – dark matter – galaxies: clusters: general

1 INTRODUCTION

According to the current paradigm of galaxy formation, all galaxies form as a result of gas cooling at the centre of the potential well of dark matter haloes. Structures form hierarchically, such that smaller haloes merge to form larger and more massive haloes. When a halo and its ‘central’ galaxy is accreted by a larger halo, it becomes a subhalo and its galaxy becomes a ‘satellite’ galaxy. In this paradigm, it is assumed that ram-pressure and tidal forces strip satellite galaxies of their gas reservoir, causing their star formation to be quenched shortly after having been accreted. The central galaxy (i.e., the galaxy with the lowest specific potential energy), however, continues to accrete new gas, and is

also expected to cannibalize some of its satellites. Consequently, it is generally assumed that the central galaxy is the most luminous, most massive galaxy in a dark matter host halo, and that it resides at rest at the centre of the halo’s potential well. Following van den Bosch et al. (2005; hereafter vdB05), we will refer to this as the ‘Central Galaxy Paradigm’ (CGP).

There are numerous areas of astronomy in which the validity of the CGP is an essential assumption, although this is rarely enunciated. Examples are various techniques to measure halo masses, such as satellite kinematics (e.g., McKay et al. 2002; van den Bosch et al. 2004; More et al. 2009), weak lensing (e.g., Mandelbaum et al. 2006; Johnston et al. 2007; Cacciato et al. 2009; Sheldon et al. 2009b), and strong lensing (e.g., Kochanek 1995; Cohn et al. 2001; Koopmans & Treu 2003; Rusin et al. 2003). In addition, the CGP also features in halo occupation modelling, where assumptions have

* E-mail: rskibba@as.arizona.edu

to be made regarding the distribution of galaxies within dark matter haloes in order to compute the galaxy-galaxy correlation function on small scales (e.g., Scoccamarro et al. 2001; Sheth et al. 2001; Yang et al. 2003; Zehavi et al. 2005; Zheng et al. 2005; Cooray 2005; van den Bosch et al. 2007; Tinker et al. 2008), and in algorithms developed to identify galaxy groups and clusters in photometric or spectroscopic redshift surveys (e.g., Yang et al. 2005a, 2007; Berlind et al. 2006; Koester et al. 2007).

Whether central galaxies actually comprise a special population has been debated for many years. However, recent analyses of galaxies in groups and clusters (e.g., Weinmann et al. 2006; Skibba et al. 2007; von der Linden et al. 2007; van den Bosch et al. 2008; Pasquali et al. 2009, 2010; Skibba 2009; Hansen et al. 2009) and halo model analyses of galaxy clustering (e.g., Skibba et al. 2006; Cooray 2006; van den Bosch et al. 2007; Skibba & Sheth 2009) have explicitly shown that central galaxies are indeed a distinct population and exhibit different properties (e.g., colour, star formation activity, AGN activity, morphology, stellar population properties) than satellite galaxies of the same stellar mass, and with different dependencies on the mass of their host halo. In addition, these studies have shown that central galaxy properties are strongly correlated with halo mass, while those of satellite galaxies only reveal a very weak dependence on the mass of the halo in which they orbit. However, it is important to realize that in virtually all of these studies, central galaxies are *assumed* to be the brightest (or most massive) halo galaxies. If this aspect of the CGP is not correct for a non-negligible fraction of all haloes, the differences between centrals and satellites found by these studies will have to be considered lower limits.

The validity of the CGP has been investigated by a number of authors. In particular, several recent, observational studies have shown that although most brightest halo galaxies (hereafter BHGs) are nearly at rest near the centroid of their group or cluster, or at the peak of the cluster X-ray emission, some of them are not (e.g., Beers & Geller 1983; Malumuth et al. 1992; Bird 1994; Postman & Lauer 1995; Zabludoff & Mulchaey 1998; Oegerle & Hill 2001; Yoshikawa et al. 2003; Lin & Mohr 2004; von der Linden et al. 2007; Bildfell et al. 2008; Hwang & Lee 2008; Sanderson et al. 2009; Coziol et al. 2009). These studies have focused on either cD galaxies in clusters, or on brightest cluster galaxies (BCGs) in general. It has been argued that most cD galaxies form a subpopulation of BCGs (e.g., Bernstein & Bhavsar 2001; Coziol et al. 2009) and may have grown by “cannibalizing” smaller neighboring galaxies.

In an early study, Beers & Geller (1983) analyzed the spatial distribution of bright galaxies in 56 rich clusters and argue that cD galaxies tend to lie at local density peaks but not necessarily at the bottom of the potential well of the whole cluster. Oegerle & Hill (2001) found that, out of their sample of 25 Abell clusters, the cD galaxies of four of them have significant peculiar velocities relative to the cluster velocity. More recent studies have analyzed the positions and velocities of BCGs. For example, in a study of 833 SDSS clusters, von der Linden et al. (2007) found that 21 BCGs in their sample lie further than 1 Mpc away from the mean galaxy in the cluster. Hwang & Lee (2008) found that the BCGs of two clusters out of a sample of 24 have significantly offset velocities and positions; these two clusters also

appear to be in dynamical equilibrium. Recently, Coziol et al. (2009), using a sample of 452 Abell clusters selected for the likely presence of a dominant galaxy, estimated that the BCGs have a median peculiar velocity of 32% of their host clusters’ radial velocity dispersion.

We emphasize that these results based on large clusters do not necessarily hold for less massive haloes. After all, in galaxy clusters, the ratio L_2/L_1 of the luminosities of the two brightest galaxies tends to be much smaller in a Milky Way (MW)-sized halo, on average (e.g., van den Bosch et al. 2007). For example, for the halo hosting the MW it is the ratio of the luminosities of the Large Magellanic Cloud and the MW, which is ~ 0.1 (van den Bergh 1999), while this ratio is much closer to unity in Virgo, Coma and other nearby clusters (Postman & Lauer 1995). Consequently, it is only natural to expect that the CGP is more likely to be valid for low mass haloes than for massive cluster-sized haloes. Nevertheless, vdB05 used a large sample of 3473 galaxy groups from the group catalogue of Yang et al. (2005a), and conclusively falsified the assumption that the brightest group galaxy is always at rest at the centre of the potential well. In this paper we extend the analysis of vdB05 using a larger, more accurate group catalogue, and focusing on different aspects of the CGP as a function of halo mass. In particular, we separately test two aspects of the CGP, namely, (i) central galaxies reside at rest at the centre of their host halo’s potential well, and (ii) central galaxies are the brightest, most massive galaxies in their host haloes. We do so by comparing three hypotheses:

- \mathcal{H}_0 : Our null hypothesis is that the CGP is correct: central galaxies are always the brightest objects in their haloes and are at rest at the centre of the potential well.
- \mathcal{H}_1 : Central galaxies are the brightest objects in their haloes, but they have a velocity and spatial offset with respect to the centre of the potential well, such that the systems still obey the Jeans equations (i.e., they are still in dynamical equilibrium). We will specify the amount of offset via a velocity bias parameter, b_{vel} , to be defined in Section 4.2.
- \mathcal{H}_2 : Central galaxies reside at rest at the centre of the potential well, but they are not the brightest objects in a fraction f_{BNC} (for ‘Brightest-Not-Central’) of all dark matter haloes.

In order to avoid confusion, throughout this paper we use the term ‘central galaxy’ to refer to the galaxy with the lowest specific potential energy. The central galaxy is the BHG in \mathcal{H}_0 and \mathcal{H}_1 , but not in \mathcal{H}_2 , and its location coincides with the centre of the halo’s potential well in \mathcal{H}_0 and \mathcal{H}_2 , but not in \mathcal{H}_1 .

We base our study on the galaxy group catalogue of Yang et al. (2007), extracted from the Sloan Digital Sky Survey (SDSS; York et al. 2000) Data Release 4 (DR4; Adelman-McCarthy et al. 2006). We analyze both the positions and velocities of BHGs relative to those of the other member galaxies, and compare the results to mock group catalogues that correspond to one of our three hypotheses. The large SDSS group catalogue, with accurate halo mass estimates, allows us to falsify \mathcal{H}_0 and to quantify the degree to which \mathcal{H}_1 and \mathcal{H}_2 are valid (i.e., to constrain the values of b_{vel} and f_{BNC}).

This paper is organized as follows. In Section 2, we

present two statistics that quantify the offsets of BHGs, and which can be used to assess deviations from the central galaxy paradigm. We describe the SDSS group catalogue in Section 3 and the construction of mock group catalogues in Section 4. In Section 5, we compare these mock catalogues to the data, in order to test our three hypotheses. We find that both \mathcal{H}_0 and \mathcal{H}_1 can be ruled out, but that \mathcal{H}_2 yields results in agreement with the data as long as $0.25 \lesssim f_{\text{BNC}} \lesssim 0.4$, with a weak dependence on halo mass. In Section 6, we discuss our results and compare them to predictions from halo occupation statistics and from two semi-analytic models of galaxy formation. We also discuss the implications for studies of satellite kinematics. Finally, we end the paper with our conclusions and a discussion of additional implications of our results.

Throughout this paper, we adopt a flat Λ CDM cosmology with $\Omega_m = 0.238$, $\Omega_\Lambda = 1 - \Omega_m$, $n = 0.951$, $\sigma_8 = 0.744$, and we express units that depend on the Hubble constant in terms of $h \equiv H_0/100 \text{ km s}^{-1} \text{ Mpc}^{-1}$. In addition, we use ‘log’ as shorthand for the 10-based logarithm.

2 PHASE-SPACE STATISTICS OF CENTRAL GALAXIES

In order to test the CGP (i.e., hypothesis \mathcal{H}_0), we use the line-of-sight velocities of galaxies obtained from their redshifts. In what follows, v_{BHG} refers to the line-of-sight velocity of the BHG, and $v_{\text{sat},i}$ refers to the line-of-sight velocity of the i^{th} satellite galaxy. We define the difference $\Delta V = \bar{v}_{\text{sat}} - v_{\text{BHG}}$ between the *mean* velocity of the satellite galaxies and that of the BHG. If the CGP is correct and $v_{\text{sat},i}$ follows a Gaussian distribution with velocity dispersion σ_{sat} , then the probability that a halo with N_{sat} satellite galaxies has a value of ΔV is given by

$$P(\Delta V)d\Delta V = \frac{1}{\sqrt{2\pi}\sigma} \exp\left[-\frac{(\Delta V)^2}{2\sigma^2}\right] d\Delta V \quad (1)$$

where $\sigma = \sigma_{\text{sat}}/\sqrt{N_{\text{sat}}}$. Therefore, in principle, one could define the parameter

$$R = \frac{\sqrt{N_{\text{sat}}}(\bar{v}_{\text{sat}} - v_{\text{BHG}})}{\sigma_{\text{sat}}}, \quad (2)$$

and test the CGP by checking whether R follows a normal distribution with zero mean and unit variance. However, the velocity dispersion σ_{sat} is generally unknown, and instead we must use its unbiased estimator

$$\hat{\sigma}_{\text{sat}} = \sqrt{\frac{1}{N_{\text{sat}} - 1} \sum_{i=1}^{N_{\text{sat}}} (v_{\text{sat},i} - \bar{v}_{\text{sat}})^2}. \quad (3)$$

Following vdB05, we use the following modified parameter as an indicator of the offset between BHGs and satellite galaxies:

$$\mathcal{R} = \frac{\sqrt{N_{\text{sat}}}(\bar{v}_{\text{sat}} - v_{\text{BHG}})}{\hat{\sigma}_{\text{sat}}}. \quad (4)$$

This parameter is similar to the relative peculiar velocities of brightest cluster galaxies, $|v_{\text{pec}}|/\sigma_{\text{cluster}}$, used in related studies (e.g., Malumuth et al. 1992; Coziol et al. 2009). If the null-hypothesis of the CGP is correct, \mathcal{R} should follow a Student t -distribution with $\nu = N_{\text{sat}} - 1$ degrees of freedom.

Note that $P_\nu(\mathcal{R})$ approaches a normal distribution with zero mean and unit variance in the limit $N_{\text{sat}} \rightarrow \infty$.

In practice, although the galaxy group finder (Yang et al. 2005a, 2007) has been thoroughly tested with mock SDSS catalogues to reliably identify galaxies residing in the same dark matter halo, it is not perfect. In particular, because of redshift errors and redshift-space distortions, the group finder inevitably selects some interlopers (galaxies that are not associated with the same halo). In addition, the SDSS suffers from various incompleteness effects. If the actual BHG is missed or misidentified, \mathcal{R} will be measured with respect to a satellite galaxy, and $|\mathcal{R}|$ will tend to be overestimated. The presence of interlopers and incompleteness effects tend to create excessive wings in the \mathcal{R} distribution, and therefore a direct comparison with the Student t -distribution cannot be made. To circumvent these problems, we compare the \mathcal{R} -distributions obtained from galaxy groups identified in the SDSS to those obtained from groups identified in mock galaxy redshift surveys (Section 4), which suffer from interlopers and incompleteness to the same extent as the real data.

We also investigate the spatial offsets of BHGs in this paper, and to do so we introduce the following parameter, analogous to the parameter \mathcal{R} , that quantifies the spatial separation between BHGs and satellite galaxies, using their projected angular separations perpendicular to the line-of-sight:

$$\mathcal{S} = \frac{\sqrt{N_{\text{sat}}}(\bar{r}_{p,\text{sat}} - r_{p,\text{BHG}})}{\hat{\sigma}_{r_{p,\text{sat}}}} \quad (5)$$

where $\bar{r}_{p,\text{sat}}$ is the mean projected position of satellite galaxies in a group, in terms of the galaxies’ mean right ascensions and declinations, and

$$\hat{\sigma}_{r_{p,\text{sat}}} = \sqrt{\frac{1}{N_{\text{sat}} - 1} \sum_{i=1}^{N_{\text{sat}}} (r_{p,\text{sat},i} - \bar{r}_{p,\text{sat}})^2}. \quad (6)$$

Both $\bar{r}_{p,\text{sat}} - r_{p,\text{BHG}}$ and $\hat{\sigma}_{r_{p,\text{sat}}}$ are expressed in h^{-1} kpc in the computation of \mathcal{S} .

For the mean and standard deviation \bar{v}_{sat} and $\hat{\sigma}_{\text{sat}}$ in the \mathcal{R} parameter (Eqn. 4), and $\bar{r}_{p,\text{sat}}$ and $\sigma_{r_{p,\text{sat}}}$ in the \mathcal{S} parameter (Eqn. 5), we have tested that other estimators for these quantities, such as the biweight estimator and the gapper (Beers et al. 1990), have an insignificant effect on our results.

Note that, with these definitions, the velocity offset \mathcal{R} and spatial offset \mathcal{S} are only valid for groups with three or more members, and are not defined for galaxy pairs or isolated galaxies.

3 APPLICATION TO THE SDSS

We first describe the SDSS galaxy group catalogue in Section 3.1 and then the subset of galaxy groups used in our analysis in Section 3.2.

3.1 Galaxy Group Catalogue

The analysis presented in this paper is based on the SDSS galaxy group catalogue of Yang et al. (2007; hereafter Y07), which is constructed by applying the halo-based group

finder of Yang et al. (2005a) to the New York University Value-Added Galaxy Catalog (NYU-VAGC; see Blanton et al. 2005), which is based on the SDSS DR4 (Adelman-McCarthy et al. 2006). From this catalogue Y07 selected all galaxies in the Main Galaxy Sample (Strauss et al. 2002) with an extinction corrected apparent magnitude brighter than $m_r = 18$, with redshifts in the range $0.01 \leq z \leq 0.20$ and with a redshift completeness $C_z > 0.7$.

This sample of galaxies is used to construct three group samples: sample I, which only uses the 362356 galaxies with measured redshifts from the SDSS, sample II which also includes 7091 galaxies with SDSS photometry but with redshifts taken from alternative surveys¹, and sample III which includes an additional 38672 galaxies that lack a redshift due to fiber collisions, but which we assign the redshift of its nearest neighbor. The present analysis is based on the galaxies in sample II with $m_r < 17.77$, which consists of 344010 galaxies.

All the magnitudes and colours of the galaxies are Petrosian, and they have been corrected for Galactic extinction (Schlegel, Finkbeiner & Davis 1998), and have been k -corrected and evolution-corrected to $z = 0.1$ (Blanton & Roweis 2007). Stellar masses for all galaxies are computed using the relations between stellar mass-to-light ratio and colour of Bell et al. (2003).

The geometry of the SDSS used for the group catalogue is defined as the region on the sky that satisfies the redshift completeness criterion. To account for the effects of the survey edges, Y07 used the SDSS DR4 survey mask with mock galaxy redshift surveys to estimate the fraction of “missing” members within the halo radius for each group. The group luminosities and masses are corrected for this fraction, and groups missing 40% or more of their members were excluded, which removes only 1.6% of all groups.

As described in Y07, the majority of the groups in our catalogue have two estimates of their dark matter halo mass: one based on the ranking of its total characteristic luminosity, and the other based on the ranking of its total characteristic stellar mass, both determined from group galaxies more luminous than $M_r - 5 \log h = -19.5$. As shown in Y07, both halo masses agree very well with each other, with an average scatter that decreases from ~ 0.1 dex at the low mass end to ~ 0.05 at the massive end. In this paper we adopt the group masses based on the stellar mass ranking, but we have checked that the luminosity ranking gives results that are almost indistinguishable. The stellar mass based group masses are available for a total of 215493 groups in our sample, which host a total of 277838 galaxies. This implies that a total of 66172 galaxies have been assigned to a group for which no reliable mass estimate is available (but see Yang, Mo & van den Bosch 2009a).

3.2 Galaxy Groups used in this Paper

In what follows we restrict our analyses to the 7234 galaxy groups in the sample II catalogue with three or more mem-

bers, with $50 \text{ km s}^{-1} \leq \hat{\sigma}_{\text{sat}} \leq 1000 \text{ km s}^{-1}$, and with reliable group masses greater than $10^{12} h^{-1} M_\odot$.

Because of the finite thickness of the spectroscopic fibers used, the SDSS suffers from incompleteness due to fiber collisions. No two fibers on the same SDSS plate can be closer than 55 arcsec. Although this fiber collision constraint is partially alleviated by the fact that neighboring plates have overlap regions, ~ 7 percent of all galaxies eligible for spectroscopy do not have a measured redshift. Since fiber collisions are more frequent in regions of high (projected) density, they are more likely to occur in richer groups, thus causing a systematic bias that may need to be accounted for. Although Sample III tries to correct for this incompleteness by assigning galaxies that lack a redshift due to fiber collisions the redshift of its nearest neighbor, Zehavi et al. (2002) have shown that in roughly 40 percent of cases, the redshift thus assigned carries a large error. Hence, although Sample II is more incomplete than Sample III, there is less of a risk of interlopers, and the redshifts are accurate, which is necessary for the analysis with galaxy line-of-sight velocities. However, if the true brightest galaxy in a group is missed due to a fiber collision, the velocity and spatial offsets \mathcal{R} and \mathcal{S} will be estimated relative to a satellite galaxy, and will tend to be overestimated, resulting in a stronger signal. To avoid this problem, we exclude groups in Sample II in which the brightest galaxy is not also a brightest group galaxy in Sample III.

This results in a sample of 6760 groups with $N_{\text{gal}} \geq 3$, excluding approximately 7% of the galaxy groups. This constitutes our fiducial galaxy group sample.² To be clear, our fiducial sample simply consists of a subset of Sample II groups. We emphasize that Sample III groups are not used in our analysis; they are only used to remove those groups from Sample II that may have been affected by fiber collisions.

In Fig. 1, we show the abundance of galaxy groups as a function of richness in the catalogue, with $M \geq 10^{12} h^{-1} M_\odot$ and $50 \text{ km s}^{-1} \leq \hat{\sigma}_{\text{rmsat}} \leq 1000 \text{ km s}^{-1}$. The requirement that the brightest group galaxy is also the brightest group galaxy in Sample III results in slightly fewer groups at all richnesses.

The analysis of vdB05 was done with a catalogue of 2502 groups in the 2dFGRS with four members or more; the new Y07 catalogue has nearly twice as many groups with $N_{\text{gal}} \geq 4$ (4571), which is a significant improvement. In addition, the typical rms redshift and magnitude errors of galaxies in the SDSS are 30 km s^{-1} and 0.035 mag (r -band), respectively (Strauss et al. 2002), compared to 85 km s^{-1} and 0.15 mag (B -band) in the 2dFGRS (Colless et al. 2001). The improved statistics of this SDSS DR4 group catalogue allow us to not only investigate the halo mass dependence of central galaxy velocity bias, but also the dependence of velocity bias on the properties of the central galaxies themselves.

¹ These redshifts are taken from the 2dFGRS (Colless et al. 2001), *IRAS* PSCz (Saunders et al. 2000), or RC3 (de Vaucouleurs et al. 1991). See Blanton et al. (2005) for details.

² Using the additional criterion that the group masses in Samples II and III are within 0.3 dex of each other excluded another 7%, but yielded results that were indistinguishable from those based on our fiducial sample.

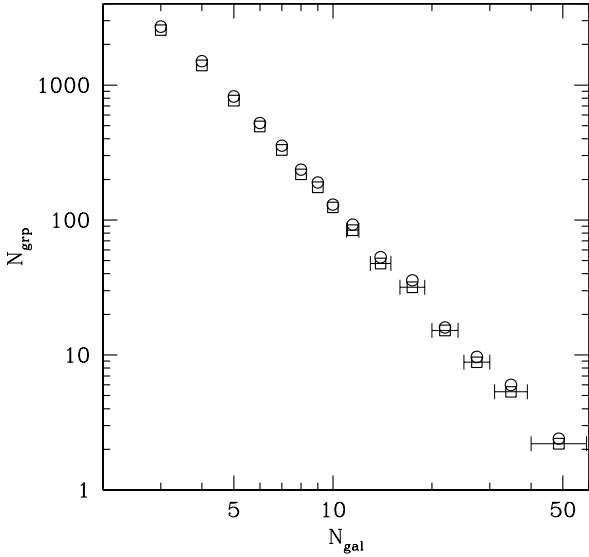


Figure 1. Galaxy group multiplicity function of SDSS Sample II. Circle points show the number of groups as a function of group richness, for groups with $M \geq 10^{12} h^{-1} M_{\odot}$ and $50 \text{ km s}^{-1} \leq \hat{\sigma}_{\text{sat}} \leq 1000 \text{ km s}^{-1}$. Square points show $N_{\text{grp}}(N_{\text{gal}})$ for groups in which we additionally require that the central galaxy is also the central galaxy of a group in Sample III. Horizontal error bars indicate the width of each bin.

4 MOCK CATALOGUES

The main goal of this paper is to use the distributions of the parameters \mathcal{R} and \mathcal{S} defined above to test our three hypotheses related to the CGP defined in Section 1. As discussed above, since the SDSS galaxy group catalogue suffers from interlopers and incompleteness effects, we require mock group catalogues constructed from mock galaxy redshift surveys (hereafter MGRSs) using the same halo-based galaxy group finder as used for the SDSS.

We construct MGRSs by populating dark matter haloes with galaxies of different luminosities. The distribution of dark matter haloes is obtained from a set of large N -body simulations (dark matter only) for the WMAP3 Λ CDM cosmology from Macciò et al. (2007). The simulations have 512^3 particles each, have periodic boundary conditions, and box sizes of $L_{\text{box}} = 100 h^{-1} \text{ Mpc}$ (hereafter L_{100}) and $L_{\text{box}} = 300 h^{-1} \text{ Mpc}$ (hereafter L_{300}). We follow Yang et al. (2004) and replicate the L_{300} box on a $4 \times 4 \times 4$ grid. The central $2 \times 2 \times 2$ boxes, are replaced by a stack of $6 \times 6 \times 6$ L_{100} boxes (see Fig. 11 in Yang et al. 2004). This stacking geometry circumvents incompleteness problems in the mock survey due to insufficient mass resolution of the L_{300} simulations, and allows us to reach the desired depth of $z_{\text{max}} = 0.20$ in all directions.

Dark matter haloes are identified using the standard FOF algorithm with a linking length of 0.2 times the mean inter-particle separation. Unbound haloes and haloes with less than 10 particles are removed from the sample. The resulting halo mass functions are in excellent agreement with the analytical halo mass function of Sheth, Mo & Tormen (2001).

4.1 Assigning Luminosities

We populate each halo with galaxies of different luminosities using the conditional luminosity function (CLF) model described in Cacciato et al. (2009; hereafter C09). The CLF, $\Phi(L|M)$, specifies the average number of galaxies of luminosity L in a halo of mass M , and is constrained to accurately match the SDSS r -band luminosity function (Blanton et al. 2003), the clustering strength of SDSS galaxies as a function of luminosity (Wang et al. 2007), and the galaxy-galaxy lensing data of Mandelbaum et al. (2006). The CLF assumes that the luminosity-dependent abundance, distribution, and clustering of galaxies can be described as a function of halo mass. The CLF of C09 is split in two parts, $\Phi_{\text{cen}}(L|M)$ and $\Phi_{\text{sat}}(L|M)$, which describe the halo occupation statistics of central and satellite galaxies, respectively.

For each halo we draw the luminosity of its central galaxy from $\Phi_{\text{cen}}(L|M)$, which is parameterized as a log-normal distribution:

$$\Phi_{\text{cen}}(L|M)dL = \frac{1}{\sqrt{2\pi} \ln(10) \sigma_{\text{cen}}} \exp \left[- \left(\frac{\log(L/L_{\text{cen}})}{\sqrt{2}\sigma_{\text{cen}}} \right)^2 \right] \frac{dL}{L}. \quad (7)$$

Here $\sigma_{\text{cen}} = 0.14$ quantifies the scatter between central galaxy luminosity and host halo mass. More et al. (2009) obtained a similar value from their analysis of satellite kinematics: $\sigma_{\text{cen}} = 0.16 \pm 0.04$. The central galaxy luminosity as a function of halo mass, $L_{\text{cen}}(M)$ is parameterized as a double power-law, with a slope of 3.3 in low-mass haloes and 0.26 in massive haloes (see C09 for details).

For the satellite galaxies we assume that their halo occupation numbers follow a Poisson distribution with mean

$$\langle N_{\text{sat}} | M \rangle = \int_{L_{\text{min}}}^{\infty} \Phi_{\text{sat}}(L|M) dL, \quad (8)$$

where we adopt a luminosity threshold, L_{min} , corresponding to $M_r - 5 \log h = -14$. The satellite luminosities are drawn from the satellite CLF $\Phi_{\text{sat}}(L|M)$, which is parameterized as a modified Schechter function:

$$\Phi_{\text{sat}}(L|M) = \frac{\phi_{\text{sat}}^*}{L_{\text{sat}}^*} \left(\frac{L}{L_{\text{sat}}^*} \right)^{\alpha_{\text{sat}}} \exp \left[- \left(\frac{L}{L_{\text{sat}}^*} \right)^s \right], \quad (9)$$

where ϕ_{sat} and α_{sat} are functions of halo mass, the parameter $s = 2$, and $L_{\text{sat}}^*(M) = 0.562 L_{\text{cen}}(M)$ (see C09 for details). We emphasize that this particular form for the CLF (eqn. 7 and 9) is not an assumption, but rather is the form that agrees with the CLF obtained directly from the SDSS group catalogue (see Yang et al. 2008). The only poorly constrained parameter is s , and we test the effect of its uncertainty in Section 6.1.

If the luminosity of the satellite is brighter than that of its central, a new luminosity is drawn until it is fainter than that of the central. Hence, in our mock universe central galaxies are always BHGs, by construction.

4.2 Assigning Phase-Space Coordinates

Having assigned all mock galaxies their luminosities, the next step is to assign them a position and velocity within their halo.

We assume that each dark matter halo of mass M has a NFW (Navarro, Frenk & White 1997) density distribution,

$\rho_{\text{dm}}(r|M)$, with virial radius $r_{\text{vir}}(M)$, characteristic scale radius $r_s(M)$, and concentration parameter $c(M) = r_{\text{vir}}/r_s$. We model the halo concentrations using the $c(M)$ relation of Macciò et al. (2007). Assuming haloes to be spherical and isotropic, the local, one-dimensional velocity dispersion follows from solving the Jeans equation

$$\sigma_{\text{dm}}^2(r|M) = \frac{1}{\rho_{\text{dm}}(r|M)} \int_r^\infty \rho_{\text{dm}}(r'|M) \frac{\partial \Psi}{\partial r}(r'|M) dr' \quad (10)$$

with $\Psi(r)$ the gravitational potential (Binney & Tremaine 1987). Using that $\partial \Psi / \partial r = GM(r)/r^2$ and defining the virial velocity $V_{\text{vir}} = \sqrt{GM/r_{\text{vir}}}$ we obtain

$$\sigma_{\text{dm}}^2(r|M) = V_{\text{vir}}^2 \frac{c}{f(c)} \left(\frac{r}{r_s} \right) \left(1 + \frac{r}{r_s} \right)^2 \mathcal{I}(r/r_s) \quad (11)$$

with $f(x) = \ln(1+x) - x/(1+x)$ and

$$\mathcal{I}(y) = \int_y^\infty \frac{f(\tau) d\tau}{\tau^3(1+\tau)^2}. \quad (12)$$

The halo-averaged velocity dispersion is given by

$$\begin{aligned} \langle \sigma_{\text{dm}} | M \rangle &\equiv \frac{4\pi}{M} \int_0^{r_{\text{vir}}(M)} \rho_{\text{dm}}(r|M) \sigma_{\text{dm}}(r|M) r^2 dr \\ &= V_{\text{vir}} \sqrt{\frac{c}{f^3(c)}} \int_0^c \frac{y^{3/2} \mathcal{I}^{1/2}(y)}{(1+y)} dy \end{aligned} \quad (13)$$

(cf. van den Bosch et al. 2004).

4.2.1 Central Galaxies

For the central galaxies, we proceed as follows. In the case of \mathcal{H}_0 and \mathcal{H}_2 mocks, we position the central galaxy at rest at the centre of the dark matter halo (for the \mathcal{H}_2 mocks, we then reshuffle the indices of central and brightest satellite, as detailed below, but we do so only after the construction of the group catalogue). In the case of the \mathcal{H}_1 mocks, we follow the approach of vdB05, to which we refer the reader for details. Briefly, we assume that the radial coordinate of the central, r , follows a probability distribution³

$$P_{\text{cen}}(r) dr = 2 \left(\frac{r_{\text{vir}} + a}{r_{\text{vir}}} \right)^2 \frac{ar}{(r+a)^3} dr, \quad (14)$$

where a is a free parameter, which is related to the velocity bias b_{vel} as detailed below. In order to parameterize the characteristic radius a in terms of that of the dark matter halo, we define the parameter $f_{\text{cen}} \equiv a/r_s$.

Central galaxies in a halo of mass M at a halo-centric radius r have an isotropic velocity dispersion

$$\begin{aligned} \sigma_{\text{cen}}^2(r|M) &= \frac{1}{\rho_{\text{cen}}(r|M)} \int_r^\infty \rho_{\text{cen}}(r'|M) \frac{\partial \Psi}{\partial r}(r'|M) dr' \\ &= V_{\text{vir}}^2 \frac{c}{f(c)} \left(\frac{r}{r_s} \right) \left(f_{\text{cen}} + \frac{r}{r_s} \right)^3 \mathcal{J}(r/r_s) \end{aligned} \quad (15)$$

with

$$\mathcal{J}(y) = \int_y^\infty \frac{f(\tau) d\tau}{\tau^3(f_{\text{cen}} + \tau)^3}. \quad (16)$$

³ The choice for this particular probability distribution, which corresponds to a Hernquist (1990) profile, is not motivated by any physical considerations, other than the fact that it is well behaved, both at $r = 0$ and at $r \rightarrow \infty$. Our results do not depend significantly on the exact shape of this probability distribution.

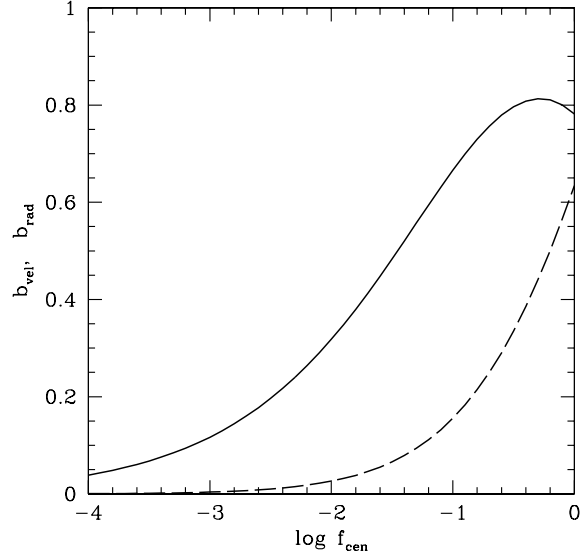


Figure 2. The velocity bias (solid curve) and spatial bias (dashed curve) of central galaxies as a function of the parameter f_{cen} , which expresses the characteristic scale of the radial distribution of central galaxies in terms of the characteristic scale of the NFW density distribution. The results shown correspond to a dark matter halo with a concentration $c = 10$.

This implies a halo-averaged velocity dispersion of

$$\begin{aligned} \langle \sigma_{\text{cen}} | M \rangle &\equiv \frac{\int_0^{r_{\text{vir}}(M)} \rho_{\text{cen}}(r|M) \sigma_{\text{cen}}(r|M) r^2 dr}{\int_0^{r_{\text{vir}}(M)} \rho_{\text{cen}}(r|M) r^2 dr} \\ &= V_{\text{vir}} \sqrt{\frac{4c}{f(c)}} f_{\text{cen}} \int_0^c \frac{y^{3/2} \mathcal{J}^{1/2}(y)}{(f_{\text{cen}} + y)^{3/2}} dy, \end{aligned} \quad (17)$$

which allows us to define the velocity bias of central galaxies as

$$b_{\text{vel}} \equiv \frac{\langle \sigma_{\text{cen}} | M \rangle}{\langle \sigma_{\text{dm}} | M \rangle} = \frac{\langle \sigma_{\text{cen}} | M \rangle}{\langle \sigma_{\text{sat}} | M \rangle}. \quad (18)$$

In addition to the velocity bias, we define the spatial bias as

$$b_{\text{rad}} \equiv \frac{\langle r_{\text{cen}} | M \rangle}{\langle r_{\text{dm}} | M \rangle} = \frac{\langle r_{\text{cen}} | M \rangle}{\langle r_{\text{sat}} | M \rangle}, \quad (19)$$

where the expectation value for the radius follows from

$$\langle r | M \rangle = \frac{\int_0^{r_{\text{vir}}} \rho(r) r^3 dr}{\int_0^{r_{\text{vir}}} \rho(r) r^2 dr} \quad (20)$$

For comparison, an NFW density distribution has $\langle r | M \rangle = 0.41 r_{\text{vir}}(M)$ for $c = 10$, and $0.47 r_{\text{vir}}(M)$ for $c = 5$.

With this model, a particular value of the parameter f_{cen} implies a particular amount of velocity and spatial bias. The relations $b_{\text{vel}}(f_{\text{cen}})$ and $b_{\text{rad}}(f_{\text{cen}})$ are shown in Figure 2. These relations only depend weakly on halo concentration (see vdB05). In the limit $f_{\text{cen}} \rightarrow 0$, the probability distribution $P_{\text{cen}}(r)$ becomes a delta function, implying that the central galaxy is sitting at rest at the centre of the dark matter halo (i.e., the null-hypothesis \mathcal{H}_0 of the CGP). Larger values of f_{cen} result in larger amounts of velocity and spatial bias. Note that b_{vel} is always larger than b_{rad} , indicating

that the signature of an off-centered central galaxy (i.e., hypothesis \mathcal{H}_1) is more pronounced, and thus easier to detect, in velocity space than in configuration space.

4.2.2 Satellite Galaxies

Throughout this paper, we assume that the N_{sat} satellite galaxies in a halo of mass M follow a number density distribution $n_{\text{sat}}(r|M) = (N_{\text{sat}}/M)\rho_{\text{dm}}(r|M)$, so that there is no spatial bias between satellite galaxies and dark matter particles. If we further assume that the satellites are in isotropic equilibrium, it also follows that there is no velocity bias between the satellites and the dark matter, neither globally [i.e., $\langle\sigma_{\text{sat}}|M\rangle = \langle\sigma_{\text{dm}}|M\rangle$] nor locally [i.e. $\sigma_{\text{sat}}(r|M) = \sigma_{\text{dm}}(r|M)$].

For simplicity, we assume that the satellites follow a spherically symmetric spatial distribution with a velocity distribution that is locally isotropic. Although this is a clear oversimplification, as some galaxy groups and clusters have anisotropic or aspherical distributions (e.g., Bailin et al. 2008; Wang et al. 2008), we do not believe that it strongly impacts our results. For example, the global velocity dispersion (i.e., obtained from all satellites) of an anisotropic system will be nearly identical to that of an isotropic system with the same gravitational potential, since both are governed by the virial equation. In other words, anisotropy changes the *local* line-of-sight velocity distribution (LOSVD), but leaves the second moment of the *global* LOSVD largely unchanged (see, e.g., van den Bosch et al. 2004). Therefore, since the \mathcal{R} parameter (eqn. 4) only depends on the first and second moments of the global LOSVD, our results are robust to the assumptions of isotropy and sphericity. The cumulative \mathcal{R} distribution is weakly dependent on higher moments of the LOSVD, but again, the effect of anisotropy is very small.

Although there is evidence to support our assumption that satellite galaxies have number density distributions that are well fit by a NFW profile (e.g., Lin et al. 2004), the corresponding concentration parameters seem to be significantly smaller than the values expected for their dark matter haloes, by about a factor of 2 to 3 (e.g., Hansen et al. 2005; Yang et al. 2005b). Since we assume that satellites are unbiased with respect to the dark matter, our value for b_{vel} will be incorrect by a factor of $\langle\sigma_{\text{sat}}\rangle/\langle\sigma_{\text{dm}}\rangle$. Using the model described in Eqs (13) and (17), we estimate that this may result in an underestimating of the velocity bias by no more than 5%. Given that this is a small effect compared to the other uncertainties involved in our analyses, we do not attempt to correct for it.

4.3 Mock Group Catalogues

Once the dark matter haloes are populated with galaxies, we construct a MGRS following the procedure described in Li et al. (2007). We place a virtual observer at the centre of the stack of simulation boxes, assign each galaxy a (α, δ) -coordinate, and remove the ones that are outside the mocked SDSS survey region. For each model galaxy in the survey region, we compute its redshift (which includes the cosmological redshift due to the universal expansion, the peculiar velocity, and a 35 km s^{-1} Gaussian line-of-sight velocity dispersion to mimic the redshift errors in the data),

and its r -band apparent magnitude (based on the r -band luminosity of the galaxy).

We eliminate galaxies that are fainter than the SDSS apparent magnitude limit, and incorporate the position-dependent incompleteness by randomly eliminating galaxies according to the completeness factors obtained from the survey masks provided by the NYU-VAGC (Blanton et al. 2005). Finally, we construct group catalogues from the MGRSs, using the same halo-based group finder as used for the real SDSS DR4.

Using the method outlined above, we construct the following set of mock group catalogues. The first is a set of ten mocks that only differ in the value of the velocity bias $b_{\text{vel}} = 0.0, 0.1, 0.2, 0.3, 0.4, 0.5, 0.6, 0.7, 0.8,$ and 1.0 . These constitute our \mathcal{H}_1 mocks. Note that the mock with $b_{\text{vel}} = 0$ satisfies the CGP, and therefore corresponds to the null-hypothesis \mathcal{H}_0 , while the other mocks correspond to \mathcal{H}_1 (i.e., BHG is central galaxy, but is not at rest at centre of dark matter potential well). The second set of mock group catalogues is constructed starting from the $b_{\text{vel}} = 0$ mock group catalogue, in which we switch the luminosities of the central and its brightest satellite for a random fraction f_{BNC} of all groups. We construct 6 mock group catalogues for $f_{\text{BNC}} = 0.1, 0.2, 0.3, 0.4, 0.5,$ and 0.6 , respectively. These constitute our \mathcal{H}_2 mocks.

In order to facilitate the comparison with the SDSS galaxy group catalogue, in what follows we discard all mock groups with an assigned group mass less than $10^{12} h^{-1} M_{\odot}$, and with a satellite velocity dispersion $\hat{\sigma}_{\text{sat}} < 50 \text{ km s}^{-1}$ or $\hat{\sigma}_{\text{sat}} > 1000 \text{ km s}^{-1}$. For the mock groups that have not been discarded, we compute the parameters \mathcal{R} and \mathcal{S} . In the next section, we compare the resulting distributions $P(< |\mathcal{R}|)$ and $P(< |\mathcal{S}|)$ with those obtained from the SDSS group catalogue in order to test our three hypotheses \mathcal{H}_0 , \mathcal{H}_1 , and \mathcal{H}_2 .

Finally, we note that the halo centres and central and satellite galaxies are defined only in the mock group catalogues, not in the SDSS group catalogue. The \mathcal{R} and \mathcal{S} parameters used in the following analysis are defined with respect to the BHGs in the mock and observed galaxy groups. This way, we are able to statistically analyze groups of a wide range in mass, including poor groups for which a centre or central galaxy might not be well-defined.

5 RESULTS

Fig. 3 shows the cumulative distributions of $|\mathcal{R}|$ (left panels) and $|\mathcal{S}|$ (right panels) obtained from the \mathcal{H}_1 mocks (upper panels) and the \mathcal{H}_2 mocks (lower panels) for groups with four or more members (i.e., $N_{\text{sat}} \geq 3$). As expected, $P(|\mathcal{R}|)$ and $P(|\mathcal{S}|)$ become broader for larger values of b_{vel} (upper panels) and f_{BNC} (lower panels). A few trends are apparent. Firstly, note that the $|\mathcal{S}|$ -distributions are all bunched together for $b_{\text{vel}} \leq 0.5$. Only for $b_{\text{vel}} > 0.5$ are the cumulative $|\mathcal{S}|$ -distributions notably different. This shows that it is difficult to constrain b_{vel} using the angular positions of galaxies, on which the \mathcal{S} -statistic is based, vis-à-vis using the velocity-statistic \mathcal{R} . Physically this is a reflection of the fact that dark matter haloes have steep potential wells, so that large velocities are required even for relatively modest excursions from the centre. Secondly, and most importantly,

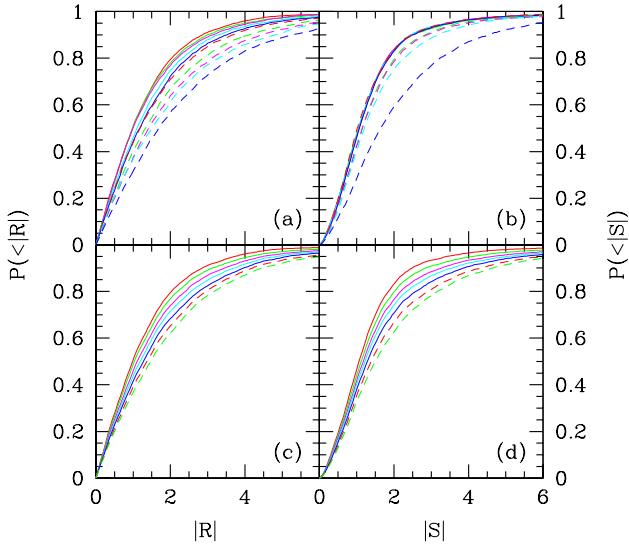


Figure 3. The cumulative distributions of $|\mathcal{R}|$ (left panels) and $|\mathcal{S}|$ (right panels) for the groups in mock group catalogues with four members or more. Upper panels show the distributions for mock catalogues with different amounts of b_{vel} : the solid curves are for $b_{\text{vel}} = 0, 0.1, 0.2, 0.3,$ and 0.4 (red, green, magenta, cyan, and blue curves, respectively) and the dashed curves are for $b_{\text{vel}} = 0.5, 0.6, 0.7, 0.8,$ and 1 (red, green, magenta, cyan, and blue curves, respectively). Lower panels show the distributions for mock catalogues with different fractions $f_{\text{BNC}} = 0, 0.1, 0.2, 0.3, 0.4, 0.5,$ and 0.6 (red, green, magenta, cyan, blue, dashed red, and dashed green curves, respectively).

Halo Mass Bins	$\log M_{\text{min}}$	$\overline{\log M}$	$\log M_{\text{max}}$	N_{group}
low mass	12	12.86	13.3	1434
intermediate mass	13.3	13.53	13.75	1540
high mass	13.75	14.09	15.2	1555

Table 1. Halo mass bins ($\log(M/h^{-1} M_{\odot})$) in the SDSS group catalogue, for groups with four members or more and $50 \text{ km s}^{-1} \leq \hat{\sigma}_{\text{sat}} \leq 1000 \text{ km s}^{-1}$. The log mass ranges, mean masses, and number of groups are given.

comparing the upper and lower panels, it is clear that a non-zero value of f_{BNC} has a different impact on $P(< |\mathcal{R}|)$ and $P(< |\mathcal{S}|)$ than a non-zero value of b_{vel} . This is good news, as it implies that we will be able to discriminate between our three hypotheses.

In what follows we will compare the cumulative $|\mathcal{R}|$ and $|\mathcal{S}|$ distributions obtained from the SDSS with those obtained from our mock catalogues. Since we have a relatively large number of groups in our SDSS sample, we can perform this test for a (small) number of bins in group mass, thus giving some leverage on a possible halo mass dependence. At the massive end of the group mass distribution, the group catalogue is roughly complete, and the mass distribution closely follows the halo mass function. The constraint of four or more group members, however, cuts off the distribution at the low mass end, leaving virtually no groups

with $M < 10^{12} h^{-1} M_{\odot}$. We split the SDSS group catalogue in three mass bins (listed in Table 1) that contain a similar number (~ 1500) of groups, and the corresponding mass cuts occur at $\log(M/h^{-1} M_{\odot}) = 13.3$ and 13.75 .

The results presented in Sections 5.1 and 5.2 are based on groups with at least four members (i.e., with $N_{\text{sat}} \geq 3$). We have repeated these analyses using samples of groups with three, five, six, and ten or more members. We have also tested lower and higher halo mass thresholds. In each case we obtain constraints on b_{vel} and f_{BNC} that are consistent with each other at the 1σ level. Hence, our results do not depend significantly on the multiplicity and halo mass thresholds used.

5.1 Testing Hypothesis \mathcal{H}_1

In order to test hypothesis \mathcal{H}_1 , we compare the SDSS group catalogue to mock group catalogues with different values of b_{vel} while setting $f_{\text{BNC}} = 0$. Figure 4a shows the cumulative $|\mathcal{R}|$ -distribution for different bins of halo mass obtained from the SDSS group catalogue (solid lines) and from three mock group catalogues corresponding to different values of b_{vel} (0, 0.5, and 1). In all cases only groups with four members or more are considered. The numbers in square brackets in each panel indicate the range of $\log(M/h^{-1} M_{\odot})$ considered. Note that at fixed \mathcal{R} , the corresponding $P(< |\mathcal{R}|)$ becomes smaller when using a bin with larger group masses. This does not necessarily imply a trend of b_{vel} with halo mass, though. It may also be due to a mass dependence of the fraction of interlopers, or a mass dependence of the completeness of group members. Indeed, the mock group samples for a fixed value of b_{vel} reveal the same trend, indicating that it is most likely an artifact introduced by the group finder. For each halo mass bin, the mock catalogue with $b_{\text{vel}} = 0$ (i.e., the one that fulfills the null-hypothesis, \mathcal{H}_0 , of the CGP) predicts a $|\mathcal{R}|$ -distribution that is much narrower than that of the SDSS, while the mock catalogue with $b_{\text{vel}} = 1$ yields a distribution that is too broad. Interestingly, the intermediate case, with $b_{\text{vel}} = 0.5$, results in $P(< |\mathcal{R}|)$ that are very similar to those of the SDSS, for each mass bin. This rules out the null hypothesis \mathcal{H}_0 , and seems to suggest that instead central galaxies have a relatively large velocity bias with $\langle \sigma_{\text{cen}} | M \rangle \simeq 0.5 \langle \sigma_{\text{sat}} | M \rangle$ with little dependence on halo mass M .

However, Fig. 4b, which is similar to Fig. 4a except that it shows the cumulative $|\mathcal{S}|$ -distributions, paints a different picture. Both the $b_{\text{vel}} = 0.0$ and $b_{\text{vel}} = 0.5$ mocks predict $|\mathcal{S}|$ -distributions that are clearly too narrow, for each mass bin. Rather, the SDSS $|\mathcal{S}|$ -distribution seems to require $0.5 < b_{\text{vel}} < 1.0$. Hence, it appears that no single value of b_{vel} can *simultaneously* match $P(< |\mathcal{R}|)$ and $P(< |\mathcal{S}|)$ obtained from the SDSS, ruling against our hypothesis \mathcal{H}_1 . In other words, although the BHGs have non-zero velocities, the velocity spread is too small to explain their displacements from the halo centres.

In order to make this more quantitative, we use the Kolmogorov-Smirnov (hereafter KS) test to compute the probabilities P_{KS} that $P(|\mathcal{R}|)$ and $P(|\mathcal{S}|)$ of the SDSS and a particular mock are drawn from the same distribution. The results are shown in Fig. 5, which plots $\log(P_{\text{KS}})$ as function b_{vel} for each of the four mass bins considered. Using the median and the 16 and 84 percentiles of $P_{\text{KS}}(b_{\text{vel}})$ for the $|\mathcal{R}|$

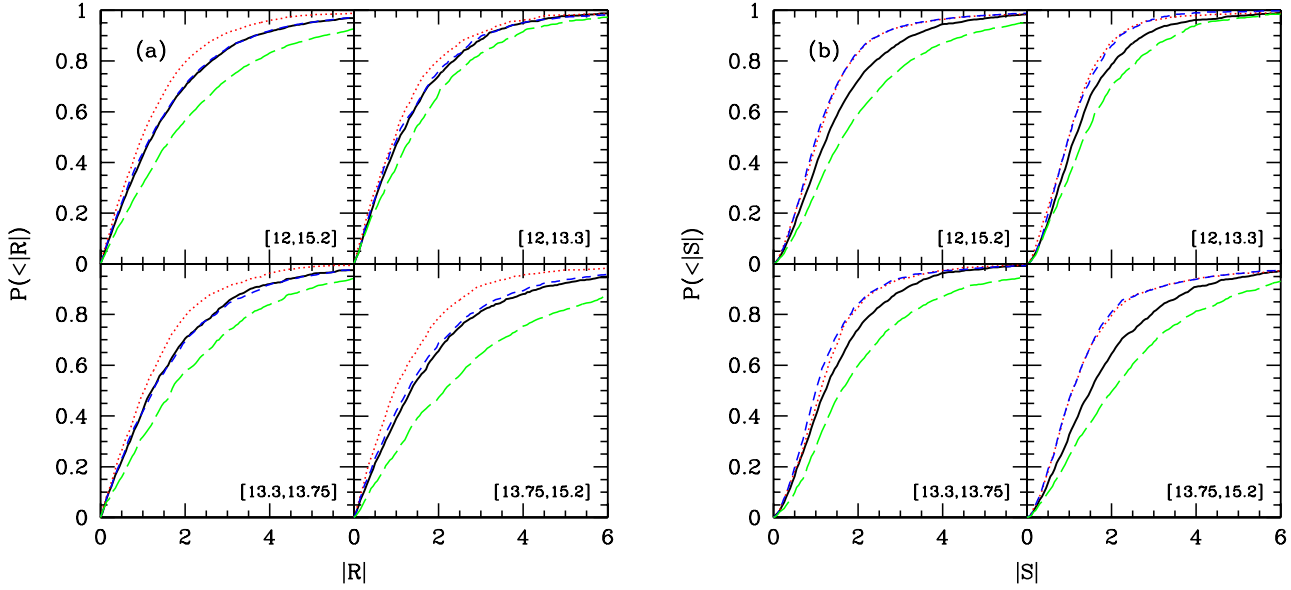


Figure 4. The cumulative distribution of $|\mathcal{R}|$ (left figure) and $|\mathcal{S}|$ (right figure) obtained from the SDSS group catalog (solid black curve) compared with those obtained from three of our mocks, with $b_{\text{vel}} = 0$ (red dotted curve), 0.5 (blue short-dashed curve), and 1 (green long-dashed curve), for groups with four members or more. Results are shown for four log halo mass intervals, as indicated in square brackets in each panel.

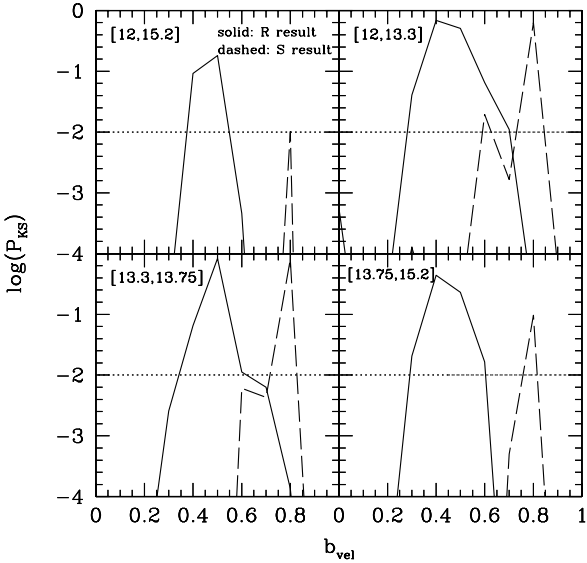


Figure 5. The KS-probability that the cumulative \mathcal{R} distribution (solid lines) and \mathcal{S} distribution (dashed lines) obtained from the SDSS groups is consistent with that obtained from our mocks, as a function of b_{vel} . Results are shown for four log halo mass intervals, indicated in square brackets in each panel. The horizontal dotted line in each panel indicates $P_{\text{KS}} = 0.01$: based on estimates of the scatter due to cosmic variance, we consider two distributions to be statistically equivalent when $P_{\text{KS}} > 0.01$.

distributions (solid lines) we obtain $b_{\text{vel}} = 0.47^{+0.06}_{-0.07}$ for the entire mass range, and $b_{\text{vel}} = 0.44^{+0.09}_{-0.07}$, $b_{\text{vel}} = 0.50 \pm 0.05$, and $b_{\text{vel}} = 0.43^{+0.08}_{-0.06}$ for the low-mass, intermediate-mass, and high-mass intervals, respectively. For the $|\mathcal{S}|$ distributions (dashed lines) this yields $b_{\text{vel}} = 0.82^{+0.08}_{-0.06}$ for the low-mass interval, and $b_{\text{vel}} = 0.83^{+0.08}_{-0.06}$ for the intermediate- and high-mass intervals. Therefore, the amounts of velocity bias consistent with the \mathcal{R} and \mathcal{S} distributions of SDSS groups are significantly different, with their best-fit values of b_{vel} differing from each other by more than 4σ . We conclude that hypothesis \mathcal{H}_1 is ruled out, since it cannot simultaneously explain the $|\mathcal{R}|$ and $|\mathcal{S}|$ distributions obtained from the SDSS group catalogue.

5.2 Testing Hypothesis \mathcal{H}_2

Having ruled out both \mathcal{H}_0 and \mathcal{H}_1 , we now turn our attention to hypothesis \mathcal{H}_2 and investigate whether there is a value of f_{BNC} for which the mock group catalogue yields $|\mathcal{R}|$ - and $|\mathcal{S}|$ -distributions that are consistent with the SDSS data. To that extent we compare the SDSS group catalogue to mock catalogues with $b_{\text{vel}} = 0$, but with different values of f_{BNC} . We proceed in the same way as for \mathcal{H}_1 in the previous section: for each mock, which corresponds to a different value of f_{BNC} , we compute $P(<|\mathcal{R}|)$ and $P(<|\mathcal{S}|)$, which we compare to the corresponding distributions obtained from the SDSS, resulting in a value for P_{KS} , the KS-probability that the mock and SDSS distributions are consistent with each other.

The results are shown in Fig. 6, where the solid and dashed lines once again correspond to the \mathcal{R} and \mathcal{S} distributions, respectively. These KS probabilities are the means of $\log(P_{\text{KS}})$ for 100 realizations with different random seeds.

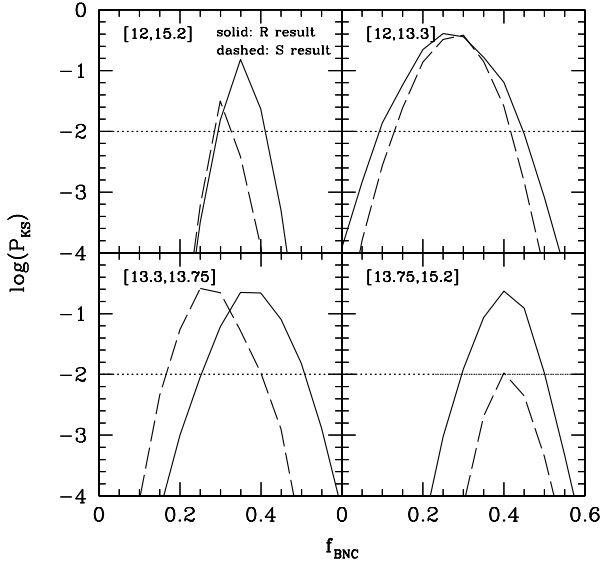


Figure 6. The KS-probability that the cumulative \mathcal{R} distribution (left figure) and \mathcal{S} distribution (right figure) obtained from the SDSS groups with four or more members is consistent with that obtained from MGRSSs, as a function of f_{BNC} , the fraction of groups in which the most luminous satellite is brighter than the central galaxy (see text for details). The KS probabilities here are the means of $\log(P_{\text{KS}})$ for 100 realizations with different random seeds.

The solid lines show that the \mathcal{R} distribution of SDSS groups indicates a relatively large fraction of groups in which the central galaxy is not the BHG, with f_{BNC} increasing from ~ 0.25 in low mass haloes ($10^{12} h^{-1} M_{\odot} \leq M \lesssim 2 \times 10^{13} h^{-1} M_{\odot}$) to ~ 0.4 in massive haloes ($M \gtrsim 5 \times 10^{13.75} h^{-1} M_{\odot}$). Interestingly, the KS probabilities obtained from the \mathcal{S} distributions shown by the dashed lines yield best-fit values of f_{BNC} that are very similar. Hence, we conclude that contrary to hypothesis \mathcal{H}_1 , hypothesis \mathcal{H}_2 can simultaneously match the $P(< |\mathcal{R}|)$ and $P(< |\mathcal{S}|)$ obtained from the SDSS group catalogue.

Fig. 7 summarizes our results. It shows the best-fit values of b_{vel} (upper panel) and f_{BNC} (lower panel) as functions of halo mass, as inferred from the $|\mathcal{R}|$ -distributions (squares) and $|\mathcal{S}|$ -distributions (triangles) obtained from the SDSS galaxy group catalogue. The figure clearly shows that \mathcal{H}_2 (i.e., a non-zero f_{BNC}) can simultaneously explain both the velocities and the positions of BHGs with respect to their satellites, while \mathcal{H}_1 (i.e., a non-zero b_{vel}) is ruled out because it cannot.

Considering the $|\mathcal{R}|$ - and $|\mathcal{S}|$ -distributions simultaneously, we infer best-fit values for the fraction of haloes in which centrals are not BHGs of $f_{\text{BNC}} = 26_{-6}^{+4}\%$ for $12 \leq \log(M/h^{-1} M_{\odot}) < 13.3$, increasing to $f_{\text{BNC}} = 30_{-4}^{+3}\%$ for haloes with $13.3 \leq \log(M/h^{-1} M_{\odot}) < 13.75$ and $f_{\text{BNC}} = 43_{-3}^{+2}\%$ in the most massive haloes with $\log(M/h^{-1} M_{\odot}) \geq 13.75$. As in Section 5.2, the best-fit values and uncertainties are determined from the median and the 16 and 84 percentiles of the $P_{\text{KS}}(f_{\text{BNC}})$ distributions.

Before proceeding with a discussion regarding the im-

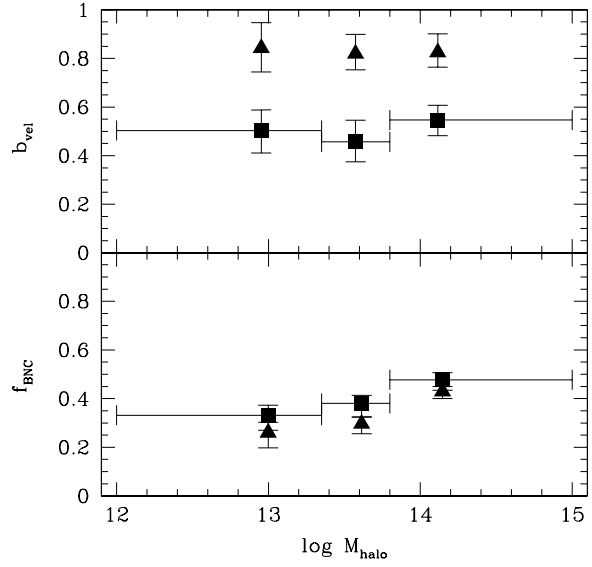


Figure 7. Halo mass dependence of b_{vel} (upper panel) and f_{BNC} (lower panel), inferred from the $|\mathcal{R}|$ -distributions (squares) and $|\mathcal{S}|$ -distributions (triangles) obtained from the analyses of the SDSS group catalogue (see text for details). For the results in the upper panel, the mock catalogues had different values of b_{vel} and $f_{\text{BNC}} = 0$; for the lower panel, the mocks had different values of f_{BNC} and $b_{\text{vel}} = 0$. Points show best-fit values of the parameters estimated from the KS probabilities, vertical error bars show $1\text{-}\sigma$ uncertainties from the 16 and 84 percentiles of the P_{KS} distributions, and horizontal error bars indicate the widths of the mass bins. Hypothesis \mathcal{H}_1 is clearly ruled out from the fact that the \mathcal{R} -data data implies a velocity bias, b_{vel} , that is inconsistent with the value inferred from the \mathcal{S} -data.

plications of these findings, we briefly address the possibility that both \mathcal{H}_1 and \mathcal{H}_2 are true; BHGs are not central galaxies in a non-zero fraction f_{BNC} of all haloes, *and* central galaxies have a non-zero value for their velocity bias b_{vel} . Using mock group catalogues with non-zero values for both f_{BNC} and b_{vel} we estimate that the data can accommodate a small amount of velocity bias $b_{\text{vel}} \lesssim 0.2$. We emphasize, though, that the data do not *require* a non-zero b_{vel} .

5.3 The Impact of Substructure

In the tests described above, we have always assumed that satellite galaxies follow a smooth, spherically symmetric, number density distribution, and we assigned the satellites peculiar velocities within its host halo under the assumption that the corresponding potential is smooth. This ignores the fact that dark matter haloes are believed to have a wealth of substructure (see Giocoli et al. 2010, and references therein; on substructure in galaxy clusters, see Richard et al. 2010). Satellite galaxies are believed to be associated with these substructures. Our treatment of the spatial and kinematic properties of satellite galaxies is only consistent with this concept of substructure if: (i) each subhalo hosts at most one satellite, and (ii) the positions and velocities of subhaloes are not correlated with those of other subhaloes. In reality, neither of these criteria is likely to be met. Massive

subhaloes are likely to host multiple satellites, and the large scale filamentary structure is believed to introduce (weakly) correlated directions of infall for subhaloes (e.g., Vitvitska et al. 2002; Aubert, Pichon & Colombi 2004; White et al. 2010). Both of these effects result in correlations among the positions and/or velocities of different satellite galaxies within the same host halo, which is likely to have an impact on the \mathcal{R} and \mathcal{S} statistics.

In order to have a crude estimate of the impact of substructure, we proceed as follows. We start by populating 1000 (virtual) dark matter haloes, all with $M = 3 \times 10^{14} h^{-1} M_{\odot}$, with galaxies using the same CLF model as in Section 4. Similar to the \mathcal{H}_0 mocks, we assure that the central galaxy is always the brightest galaxy in the halo, and we position it at rest at the centre of the halo. We then compute \mathcal{S} and \mathcal{R} for each of these haloes. The black, solid lines in Fig. 8 indicate the corresponding $P(< |\mathcal{R}|)$ and $P(< |\mathcal{S}|)$. Next we repeat this exercise, but now, in each halo, a fraction f_{sub} of all satellites is ‘clumped’ together in a single substructure. We model this substructure as a halo of mass $m = f_{\text{sub}}M$ (i.e., we assign the galaxies in this subhalo phase-space coordinates in exactly the same way as we would if the halo was a ‘host’ halo of the same mass). The phase-space coordinates of the centre of the subhalo are drawn in the same way as the phase-space coordinates of the satellites that are not in a substructure. The long-dashed green curves, short-dashed blue curves, and dotted red curves in Fig. 8 show the $P(< |\mathcal{R}|)$ and $P(< |\mathcal{S}|)$ thus obtained for $f_{\text{sub}} = 1/3$, $1/5$, and $1/10$, respectively. A comparison with the no-substructure case (black, solid line) shows that substructure significantly affects the \mathcal{R} and \mathcal{S} distributions, and hence our conclusions, if *all* dark matter haloes have a most massive substructure whose mass is $m_{\text{sub}} \gtrsim 0.1M$. In particular, if many haloes contain substantial substructure, then an alternative explanation for the fact that our fiducial model (which follows the CGP) does not match the data may be that the phase-space coordinates of satellite galaxies within the same dark matter host halo are correlated. In that case the fractions f_{BNC} obtained in Section 5.2 will be significantly overestimated.

However, using the subhalo mass functions of Giocoli et al. (2010), we estimate that only $\sim 8\%$ of host haloes with $M = 3 \times 10^{14} h^{-1} M_{\odot}$ have a most massive subhalo with $f_{\text{sub}} = m/M \geq 0.1$, while only ~ 0.7 percent have a most massive subhalo with $m/M \geq 0.3$. Based on these estimates, and on the tests described above, we argue that ignoring substructure when populating haloes with (satellite) galaxies does *not* have a significant impact on the \mathcal{R} and \mathcal{S} statistics, though more sophisticated tests are required to confirm this. Therefore, we conservatively argue that the f_{BNC} fractions obtained in this paper have to be regarded as upper limits.

6 DISCUSSION

The results presented in the previous section suggest that in as much as 25 to 40 percent of all haloes, the brightest galaxy is a satellite rather than a central galaxy. In order to put these numbers in perspective, we compare them to predictions from halo occupation statistics (Section 6.1) and from two semi-analytical models of galaxy formation

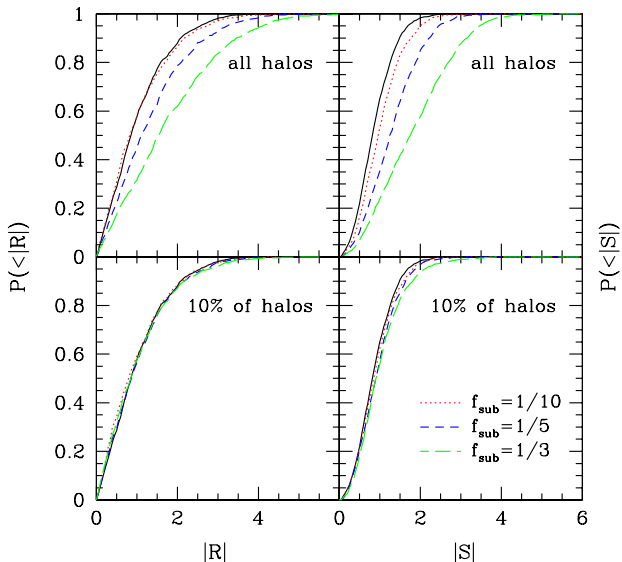


Figure 8. Cumulative distributions of $|\mathcal{R}|$ (left panels) and $|\mathcal{S}|$ (right panels) of 1000 mock haloes with $M = 3 \times 10^{14} h^{-1} M_{\odot}$ populated with galaxies. Black solid curves indicate the distributions for haloes with no substructure, while the long-dashed green curves, short-dashed blue curves, and dotted red curves indicate the distributions for $f_{\text{sub}} = 1/3$, $1/5$, and $1/10$, respectively. Results are shown for the case in which all haloes have substructure (upper panels) and 10% of the haloes have substructure (lower panels).

(Section 6.2). We also investigate the impact of non-zero $f_{\text{BNC}}(M)$ on the halo masses inferred using satellite kinematics (Section 6.3).

6.1 Comparison with Halo Occupation Statistics

Using the SDSS r -band luminosity function of Blanton et al. (2003), the projected two-point correlation functions of Wang et al. (2007), and the galaxy-galaxy lensing data of Mandelbaum et al. (2006), C09 constrained the halo occupation statistics as parameterized by the conditional luminosity function (CLF)

$$\Phi(L|M) = \Phi_{\text{cen}}(L|M) + \Phi_{\text{sat}}(L|M), \quad (21)$$

which is found to be in good agreement with direct constraints from the Y07 group catalogue (Yang, Mo & van den Bosch 2008, 2009a) and with constraints from satellite kinematics (More et al. 2009). We have used this CLF model in Section 4.1 to construct our mock group catalogues, except that we imposed that the central galaxy is always the BHG; if a satellite luminosity was drawn from $\Phi_{\text{sat}}(L|M)$ that was brighter than the central luminosity, drawn from $\Phi_{\text{cen}}(L|M)$, it was rejected. Later, we then switched the luminosities of the central and that of its brightest satellite in a fraction f_{BNC} of all groups. We now use the CLF to ‘predict’ the fraction f_{BNC} as function of halo mass, by making the assumption that the luminosities of satellite galaxies are independent of the luminosity of the central galaxy in the same halo. In that case, the probability that a random satel-

lite galaxy in a halo of mass M has a luminosity smaller than that of its central is simply given by

$$P(L_{\text{sat}} < L_{\text{cen}}|M) = \int_0^\infty \frac{\int_{L_{\text{min}}}^{L_{\text{cen}}} \Phi_{\text{sat}}(L|M) dL}{\int_{L_{\text{min}}}^\infty \Phi_{\text{sat}}(L|M) dL} \Phi_{\text{cen}}(L_{\text{cen}}|M) dL_{\text{cen}}, \quad (22)$$

where the integral accounts for the scatter in the relationship between central galaxy luminosity and halo mass, and L_{min} is the minimum luminosity considered. In a halo with N_{sat} satellites, the probability that the central galaxy is also the brightest galaxy is simply $[P(L_{\text{sat}} < L_{\text{cen}}|M)]^{N_{\text{sat}}}$. Hence, we obtain that

$$f_{\text{BNC}}(M) = 1 - \sum_{N_{\text{sat}}=1}^{\infty} P(N_{\text{sat}}|M) [P(L_{\text{sat}} < L_{\text{cen}}|M)]^{N_{\text{sat}}} \quad (23)$$

where $P(N_{\text{sat}}|M)$ gives the probability that a halo of mass M contains N_{sat} satellites, which we take to be a Poisson distribution whose mean is given by Eqn. (8). The results thus obtained from the CLF of C09 are shown as a solid line in Fig. 9. For comparison, the solid triangles with error bars are the constraints on $f_{\text{BNC}}(M)$ obtained from the SDSS group catalogue as described in the previous section. Although the CLF predicts that f_{BNC} increases with increasing halo mass, in qualitative agreement with the data, the values of $f_{\text{BNC}}(M)$ inferred from the data are much larger than those ‘predicted’ by the CLF. Note that the CLF prediction is for *all* haloes, rather than for haloes (or groups) with $N_{\text{sat}} \geq 3$, which is the richness threshold used in our analysis of SDSS groups. However, this has little to no impact. We have verified that our constraints on f_{BNC} do not change significantly if we use a different richness threshold. Furthermore, from the CLF, the probability of a halo hosting fewer than three galaxies is low for most of the mass range considered here: $P(N_{\text{sat}} < 3) > 0.05$ only for haloes with $\log M < 12.75$.

There are a number of possible explanations for why the CLF prediction is not consistent with the data. First of all, we emphasize that the CLF is not designed to ‘predict’ $f_{\text{BNC}}(M)$. Most of the statistics used to constrain the CLF depend only very weakly (clustering and lensing) or not at all (luminosity function) on $f_{\text{BNC}}(M)$. Secondly, it is still possible that the CLF is correct, but that the additional assumption that the satellite luminosity is independent of the luminosity of the central is not correct, that is, $\Phi_{\text{sat}}(L_{\text{sat}}|M, L_{\text{cen}}) \neq \Phi_{\text{sat}}(L_{\text{sat}}|M)$. This could come about, for example, because of galactic ‘cannibalism’: those haloes in which the central has recently cannibalised a bright satellite will have an excessively bright central, and are less likely to have a bright satellite. It remains to be seen whether a model for $\Phi_{\text{sat}}(L_{\text{sat}}|M, L_{\text{cen}})$ can be found that yields a $f_{\text{BNC}}(M)$ in better agreement with the data, and simultaneously obeys the CLF constraint that

$$\Phi_{\text{sat}}(L_{\text{sat}}|M) = \int \Phi_{\text{sat}}(L_{\text{sat}}|M, L_{\text{cen}}) \Phi_{\text{cen}}(L_{\text{cen}}|M) dL_{\text{cen}}. \quad (24)$$

Of course, it is also possible that the discrepancy reflects an actual failure of the CLF. One possible modification, which will have little impact on the luminosity function, clustering, galaxy-galaxy lensing, and mock group catalogues, is a modification in the shape of $\Phi_{\text{sat}}(L|M)$ (eqn. 9)

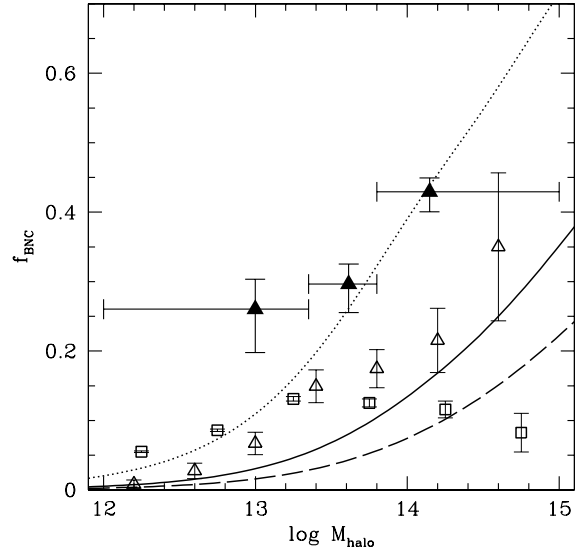


Figure 9. Probability that the most luminous satellite galaxy is brighter than the central galaxy in a halo, as a function of halo mass (Eqn. 23). Result is shown for three slopes in the satellite CLF (Eqn. 9): $s = 1$ (dotted curve), the fiducial $s = 2$ (solid curve), and $s = 3$ (dashed curve). For comparison, the $f_{\text{BNC}}(M_{\text{halo}})$ result from Figure 7 (solid triangle points) is also shown. The predictions from the MORGANA semi-analytic model (open triangles) and Croton et al. (2006) semi-analytic model (open squares) are also shown, with Poisson errors.

at the bright end. As mentioned in Section 4.1, C09 adopted a functional form for which $\Phi_{\text{sat}}(L|M) \propto \exp[-(L/L_{\text{sat}}^*)^s]$ at the bright end, with $s = 2$. The exact value of s , though, is poorly constrained by the data, but has a significant impact on $f_{\text{BNC}}(M)$. This is illustrated by the dotted and dashed curves in Fig. 9, which correspond to $s = 1$ and $s = 3$, respectively. Clearly, decreasing s increases the expectation value for the luminosity of the brightest satellite, and hence the fraction of haloes for which the central galaxy is not the BHG. For $s = 1$ the CLF ‘predicts’ a $f_{\text{BNC}}(M)$ in good agreement with the data, but only for $M \gtrsim 5 \times 10^{13} h^{-1} M_{\odot}$. For less massive haloes, the value of f_{BNC} inferred from the SDSS group catalogue is still too high compared to the CLF prediction, but only by about 2σ .

Another parameter that has a significant impact on $f_{\text{BNC}}(M)$ is the ratio $Q \equiv L_{\text{sat}}^*/L_{\text{cen}}$. Motivated by the CLF inferred from the SDSS group catalogue by Yang et al. (2008), C09 adopted $Q = 0.562$, with no dependence on halo mass. However, Hansen et al. (2009), using the maxBCG group catalogue of Koester et al. (2007), found that Q depends on halo mass and may be as small as ~ 0.15 for $M \sim 10^{14} h^{-1} M_{\odot}$. In order for the CLF to yield $f_{\text{BNC}}(M)$ in rough agreement with our findings, though, we need a value of Q that is *larger* than 0.562, (i.e., for $s = 2$ we require $Q \sim 0.7$). These results warrant a more thorough investigation into the exact values of s and Q as function of halo mass.

Finally, we have verified that the CLF predictions for

$f_{\text{BNC}}(M)$ do not depend significantly on our choice for the lower luminosity cut-off, L_{min} .

6.2 Comparison with Semi-Analytical Models

We now compare our results to the predictions of two semi-analytical models (SAMs) of galaxy formation; the MOR-GANA model of Monaco, Fontanot & Taffoni (2007), as updated by Lo Faro et al. (2009), and the SAM of Croton et al. (2006).

Both SAMs adopt flat Λ CDM cosmologies, albeit with slightly different values for the cosmological parameters⁴. Although both SAMs include treatments of cooling, star formation, feedback from supernovae and active galactic nuclei, mergers, starbursts and disk instabilities, the actual implementations of these physical processes are substantially different (see the original papers for details). Yet, as shown in Fig. 9 (open symbols), they predict fairly similar values for $f_{\text{BNC}}(M)$.⁵ In qualitative agreement with the data, both SAMs predict that f_{BNC} increases with halo mass. In addition, from studying the satellite BHGs in the MORGANA model, we find that the majority of the more massive satellites represent a recently (since $z \sim 0.2$) accreted population, in most cases linked to the last major merger experienced by the host halo. In other words, infalling massive satellites could be a contributing cause of a nonzero f_{BNC} .

As with the halo occupation statistics, the predictions of both models are significantly lower than the data. In both SAMs, satellite galaxies are ‘strangulated’ after being accreted by their host galaxies, so that they do not participate in the cooling flow of their parent halo. However, it has been pointed out that the standard, instantaneous implementation of this strangulation causes an over-quenching of satellite galaxies (e.g., Baldry et al. 2006; Weinmann et al. 2006; Kimm et al. 2009). It has been suggested that this over-quenching problem can be avoided by adopting a longer time-scale for strangulation (e.g., Kang & van den Bosch 2008; Font et al. 2008; Weinmann et al. 2009). This is likely to allow satellite galaxies to continue forming stars for some period, which will increase their stellar mass, and thus also f_{BNC} . The effect, though, is likely to be small. Another effect that may cause the SAMs to underpredict f_{BNC} is the fact that they often adopt dynamical friction time-scales that are too short (Boylan-Kolchin et al. 2008; Wetzel & White 2010). This results in (massive) satellites being accreted too rapidly, and hence in an underestimate of f_{BNC} . Finally, the models don’t take proper account of stellar mass stripping due to tidal forces, which will make satellites *less* massive. As emphasized in a number of recent papers, this tidal stripping of satellite galaxies is an important ingredient of galaxy formation (Monaco et al. 2006; White et al. 2007; Conroy, Ho & White 2007; Conroy, Wechsler & Kravtsov 2007; Kang & van den Bosch 2008; Yang, Mo & van den Bosch 2009b; Pasquali et al. 2010). It remains to be seen

⁴ We do not believe that these small differences will have a significant impact on the predictions of $f_{\text{BNC}}(M)$.

⁵ As in our analysis of SDSS galaxy groups, the predictions of $f_{\text{BNC}}(M)$ from the SAMs are the fractions of haloes in which a satellite galaxy is the most luminous galaxy. The SAMs’ predictions are almost exactly same for the fractions of haloes in which a satellite is the most massive galaxy (in terms of stellar mass).

to what extent these additions and/or modifications of the semi-analytical models impact $f_{\text{BNC}}(M)$. For the moment, we conclude that the $f_{\text{BNC}}(M)$ inferred from our analysis of SDSS galaxy groups is uncomfortably high compared to predictions from both halo occupation statistics and from semi-analytical models of galaxy formation.

6.3 Implication for Satellite Kinematics

Studies that attempt to infer the masses of dark matter haloes using the kinematics of satellite galaxies always assume that the CGP is valid (e.g., Zaritsky et al. 1993; McKay et al. 2002; van den Bosch et al. 2004; More et al. 2009). Since a typical central only has a few satellites, one normally stacks many centrals together in order to obtain sufficient signal-to-noise to measure a reliable satellite velocity dispersion, σ_{sat} . With sufficiently large galaxy redshift surveys, one can measure σ_{sat} as a function of the luminosity (or stellar mass) of the central galaxies (i.e., one stacks centrals in narrow bins in luminosity or stellar mass).

Consider a halo with N_{sat} satellites with velocities $v_{\text{sat},i}$ with respect to halo centre, and let the central be stationary at the centre of the halo (i.e., $v_{\text{cen}} = 0$). The satellite velocity dispersion measured with respect to the central is:

$$\sigma_{\text{true}}^2 = \frac{1}{N_{\text{sat}}} \sum_{i=1}^{N_{\text{sat}}} v_{\text{sat},i}^2. \quad (25)$$

Without loss of generality, assume that satellite number 1 is misidentified to be the central. The *measured* velocity dispersion in this case will be:

$$\sigma_{\text{meas}}^2 = \frac{1}{N_{\text{sat}}} \left[\sum_{i=2}^{N_{\text{sat}}} (v_{\text{sat},i} - v_{\text{sat},1})^2 + (v_{\text{cen}} - v_{\text{sat},1})^2 \right] \quad (26)$$

The first term sums over the remaining $N_{\text{sat}} - 1$ true satellites, while the last term is the contribution from the true central. Using that $\langle v_{\text{sat},i} \rangle = 0$, and that $\langle v_{\text{cen}} \rangle = \langle v_{\text{cen}}^2 \rangle = 0$, it is easy to show that the velocity dispersion measured from a stack of many systems, each with N_{sat} satellites, is equal to

$$\frac{\sigma_{\text{meas}}^2}{\sigma_{\text{true}}^2} = 1 + f_{\text{BNC}} (1 - N_{\text{sat}}^{-1}), \quad (27)$$

where f_{BNC} is the fraction of systems in which the central is misidentified. Note that when the number of satellites per central is one, the measured velocity dispersion is identical to the true one, independent of f_{BNC} , that is, the fact that some satellites are misidentified as centrals has no impact on the inferred satellite kinematics.⁶ However, in the limit $N_{\text{sat}} \rightarrow \infty$, one has that $\sigma_{\text{meas}} = \sqrt{1 + f_{\text{BNC}}} \sigma_{\text{true}}$. Since the inferred halo mass $M \propto \sigma_{\text{sat}}^3$, this implies that the mass of the halo will be overestimated by a factor $(1 + f_{\text{BNC}})^{3/2}$. Note that Eqn. (27) is strictly valid only for stacks of systems that all have the same number of satellites. In reality, however, there will be scatter in the number of satellites per host in the stack. In what follows we assume that we do not make a large error if we adopt Eqn. (27) but with N_{sat} replaced by the *average* number of satellites per central, $\langle N_{\text{sat}} \rangle$.

⁶ This statement ignores the fact that a non-zero f_{BNC} also impacts the interpretation of the stacking parameter (i.e., the luminosity of the alleged ‘centrals’) and may result in more interlopers.

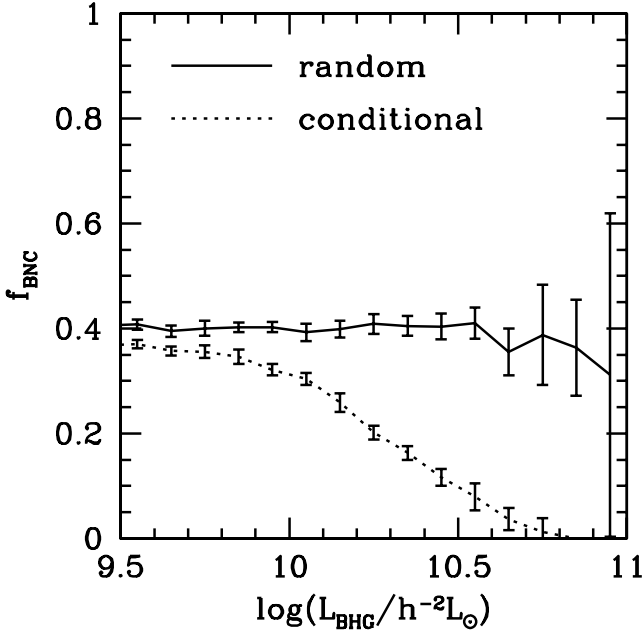


Figure 10. Fraction f_{BNC} of haloes in which the brightest galaxy is not the central one, as a function of the luminosity of the brightest halo galaxy. The solid line shows $f_{\text{BNC}}(L_{\text{BHG}})$ for the ‘random’ mocks, and the dotted line shows the fraction for the ‘conditional’ mocks, in which whether a halo has a satellite brighter than the central is conditional on the luminosity of the central galaxy. The luminosities correspond to r -band absolute magnitudes, such that $\log L = 9.5$ corresponds to $M_r \approx -19$, and $\log L = 10.3$ to $M_r \approx -21$, etc.

For relatively faint centrals, $\langle N_{\text{sat}} \rangle \simeq 1$, and $\sigma_{\text{meas}} \simeq \sigma_{\text{true}}$ independent of the value of f_{BNC} . However, at the bright end $\langle N_{\text{sat}} \rangle$ becomes substantially larger than unity, and a non-zero f_{BNC} may cause a significant overestimate of the true σ_{sat} . For example, in their analysis of satellite kinematics, More et al. (2009) have $\langle N_{\text{sat}} \rangle \sim 10$ for their brightest host bins. If f_{BNC} for these bins is comparable to $f_{\text{BNC}}(M)$ at the massive end, (i.e., $f_{\text{BNC}} \sim 0.4$), their inferred halo masses around bright host galaxies will be overestimated by a factor ~ 1.6 .

However, since the halo mass luminosity relation for central galaxies is not one-to-one, it is not trivial to infer f_{BNC} for a certain bin in host galaxy luminosity, L_{host} , from $f_{\text{BNC}}(M)$. In fact, one can construct mocks in which $f_{\text{BNC}}(L_{\text{host}})$ is very small at the bright end, even when $f_{\text{BNC}}(M)$ is large at the massive end, by making the criterion for a halo having a satellite brighter than the central conditional on the luminosity of the central galaxy. We illustrate a particular case of this in Fig. 10, where we show $f_{\text{BNC}}(L_{\text{BHG}})$ for two types of mocks that have identical $f_{\text{BNC}}(M) = 0.4$. These are constructed as follows. We start by populating the dark matter haloes in our $100h^{-1}$ Mpc simulation box described in Section 4 with galaxies of different luminosities using the CLF of C09 (see Section 4.1 for details). If the luminosity of a satellite is brighter than that of its central, a new luminosity is drawn until it is fainter than that of the central, so that $f_{\text{BNC}} = 0$. For the first set of mocks, we switch the luminosities of the central and that of its brightest satellite in a random fraction of 40 percent of all haloes, and we measure the resulting $f_{\text{BNC}}(L_{\text{BHG}})$. We refer to these

as the ‘random’ mocks. The mean and scatter obtained from ten realizations are shown as the solid line in Fig. 10. As expected, $f_{\text{BNC}}(L_{\text{BHG}}) \simeq 0.4$, independent of L_{BHG} . For the second set of mocks, we again start from the mocks with $f_{\text{BNC}} = 0$, but we now switch the luminosities of brightest satellite and central in those haloes that meet the criterion

$$\int_0^{L_{\text{cen}}} \Phi_{\text{cen}}(L|M) dL < 0.4, \quad (28)$$

that is, in those haloes in which the luminosity of the central falls in the lower 40 percentile of its distribution, $\Phi_{\text{cen}}(L|M)$. We refer to these as the ‘conditional’ mocks, and similar to the ‘random’ mocks they thus have $f_{\text{BNC}}(M) = 0.4$. Yet, their $f_{\text{BNC}}(L_{\text{BHG}})$, indicated by the dotted curve in Fig. 10, are very different: they decrease from ~ 0.4 at the faint end to almost zero at the bright end. Hence, if the probability that a central is not the BHG is conditional on the luminosity of the central, which seems to be a reasonable assumption, then even a relatively large $f_{\text{BNC}}(M)$ may have negligible impact on the halo masses inferred from satellite kinematics.

We thus conclude that a proper assessment of the impact of a non-zero $f_{\text{BNC}}(M)$ on the halo masses inferred from satellite kinematics requires an independent assessment of the fraction f_{BNC} as function of the luminosities of the host galaxies.

7 CONCLUSIONS

It is generally assumed that the central galaxy in a dark matter halo, that is, the galaxy with the lowest specific potential energy, is also the brightest halo galaxy (BHG) and that it resides at rest at the centre of the dark matter potential well. This central galaxy paradigm (CGP) is an essential assumption made in various fields of astronomical research (e.g., satellite kinematics, gravitational lensing, both weak and strong, halo occupation modelling).

In this paper, we have used a large galaxy group catalogue, constructed from the SDSS DR4 by Yang et al. (2007), in order to test the validity of the CGP. For each group we compute two statistics, \mathcal{R} and \mathcal{S} , which quantify the offsets of the line-of-sight velocities and projected positions of brightest group galaxies relative to the other group members. By comparing the cumulative distributions of $|\mathcal{R}|$ and $|\mathcal{S}|$ to those obtained from detailed mock group catalogues, we have tested the null-hypothesis, \mathcal{H}_0 , that the CGP is correct; hypothesis \mathcal{H}_1 , according to which central galaxies are BHGs but have a non-zero velocity with respect to the halo centre, parameterized by a non-zero velocity bias, b_{vel} ; and hypothesis \mathcal{H}_2 , according to which central galaxies reside at rest at the centre of the halo’s potential well, but are not the BHGs in a fraction f_{BNC} of all haloes.

In agreement with vdB05, who only used the \mathcal{R} statistic, we show that the null-hypothesis is strongly ruled out. However, contrary to vdB05, who argued that the data are consistent with a non-zero b_{vel} , we show that \mathcal{H}_1 fails to *simultaneously* match the $|\mathcal{R}|$ and $|\mathcal{S}|$ distributions⁷. Rather,

⁷ Since vdB05 did not consider the spatial offsets (i.e., the \mathcal{S} statistic), they were unable to notice this problem for the \mathcal{H}_1 hypothesis.

we have shown that the data is consistent with hypothesis \mathcal{H}_2 , indicating that BHGs are not central galaxies in a non-negligible fraction of all haloes; in particular, we find that f_{BNC} increases from ~ 0.25 in low mass haloes ($10^{12} h^{-1} M_{\odot} \leq M \lesssim 2 \times 10^{13} h^{-1} M_{\odot}$) to ~ 0.4 in massive haloes ($M \gtrsim 5 \times 10^{13} h^{-1} M_{\odot}$).

Considering combined models, in which BHGs are not central galaxies in a non-zero fraction f_{BNC} of all haloes, and central galaxies have a non-zero value for their velocity bias b_{vel} , we find that the data can at most accommodate a small amount of velocity bias ($b_{\text{vel}} \lesssim 0.2$). We emphasize, though, that a non-zero velocity bias is not *required* by the data (see vdB05 for a discussion of possible physical explanations for a non-zero b_{vel}).

Our main result is that the fraction f_{BNC} is significant and increases with halo mass. Since some authors have assumed that the most luminous (or most massive) galaxy in a system is the central galaxy, our result that f_{BNC} is somewhat large in galaxy groups and larger ($43^{+2}_{-3}\%$) in more massive clusters may seem surprising. Nevertheless, our results are consistent with other studies. For example, von der Linden et al. (2007) find that in 343 of their 625 clusters ($\approx 55\%$), the identified BCG is not the ‘mean’ galaxy (which lies at the centre of the cluster’s density field). Coziol et al. (2009) find that in about half of their 452 clusters, the BCGs have a median peculiar velocity greater than one third of their clusters’ velocity dispersion. Finally, in the Local Group, although the Milky Way and Andromeda both have their own systems of satellites, they could be considered part of a single group, in which Andromeda would be identified as the BHG (van den Bergh 1999). The two galaxies are expected to eventually merge, although neither is clearly the ‘central’ galaxy.

In order to put our constraints on $f_{\text{BNC}}(M)$ in perspective, we have compared them to predictions from semi-analytical models (SAMs) for galaxy formation and from halo occupation statistics. Both the SAM of Croton et al. (2006) and that of Lo Faro et al. (2009) predict $0.1 \lesssim f_{\text{BNC}} \lesssim 0.2$ in the halo mass range of $10^{13} h^{-1} M_{\odot} \lesssim M \lesssim 10^{15} h^{-1} M_{\odot}$, significantly lower than the $f_{\text{BNC}}(M)$ inferred here from our SDSS galaxy group catalogue.

We can also use the CLF model of C09 to predict $f_{\text{BNC}}(M)$, if we assume that the luminosity of a satellite galaxy is independent of the luminosity of its corresponding central. Although the C09 halo occupation model accurately matches the SDSS r -band luminosity function of Blanton et al. (2003), the projected two-point correlation functions of Wang et al. (2007), and the galaxy-galaxy lensing data of Mandelbaum et al. (2006), this model also predicts a $f_{\text{BNC}}(M)$ that is far too low. We have shown that one can increase the predicted $f_{\text{BNC}}(M)$ using some small modifications of the CLF, but it remains to be seen how these modifications impact the clustering and lensing predictions. For completeness, we emphasize that halo occupation models based on the abundance-matching method (e.g., Vale & Ostriker 2004; Conroy, Wechsler & Kravtsov 2006, 2007; Shankar et al. 2006; Guo et al. 2010; Moster et al. 2010) ‘predict’ that $f_{\text{BNC}} = 0$, by construction, unless they assume a non-zero scatter in the relation between central galaxy luminosity and halo mass. Typically a larger amount of scatter will imply a larger f_{BNC} . It remains to

be seen whether the amount of scatter required to match the $f_{\text{BNC}}(M)$ inferred here is consistent with independent constraints, such as those obtained from satellite kinematics (More et al. 2009). All in all, we conclude that the constraints on $f_{\text{BNC}}(M)$ obtained in this paper are uncomfortably high compared to predictions from galaxy formation models and halo occupation statistics. One possible explanation may be that dark matter haloes have substructure, something that we have ignored in our analysis. Although simple tests suggest that the correlations in the phase-space parameters of satellite galaxies due to substructure are not strong enough to significantly impact our conclusions, we caution that more detailed studies are required to confirm this.

Our results have important implications for various areas in astrophysics. In particular, we have shown that a non-zero f_{BNC} may cause an overestimate of halo masses inferred from satellite kinematics. Although the effect is expected to be negligible for faint host galaxies, because they typically only have of the order of one satellite per host, the overestimate can be significant at the bright end. The exact impact, though, depends on the fraction f_{BNC} as function of the host luminosity, which may be very different from that as a function of halo mass. For example, if BHGs are not centrals in the fraction $f_{\text{BNC}}(M)$ of haloes of mass M that host the faintest centrals, then $f_{\text{BNC}}(L)$ drops towards zero at the bright end, and the impact on satellite kinematics is negligible.

Additional methods and analyses that may be affected by a non-zero f_{BNC} are the following:

- The inference of halo masses from weak gravitational lensing. Similar to satellite kinematics, weak lensing studies often rely on stacking the lensing signals of many clusters and groups binned by mass-correlated observables such as richness and luminosity. When interpreting such data, it is generally assumed that BHGs coincide with the centres of the dark matter haloes (e.g., Mandelbaum et al. 2006; Johnston et al. 2007; Sheldon et al. 2009a,b; Corless & King 2009; C09). Since satellite galaxies yield a different lensing signal than centrals, at least on small to intermediate scales (see e.g., Yang et al. 2006), a non-zero f_{BNC} may have a significant impact on the lensing signal (Johnston et al. 2007), by resulting in underestimates of the richnesses and lensing profiles, for example. C09 used the CLF described in Section 4.1 to model the galaxy-galaxy lensing signal of Mandelbaum et al. (2006). As shown in Section 6.1, this CLF predicts $f_{\text{BNC}}(M)$ significantly lower than inferred here. It remains to be seen to what extent this may affect their interpretation of the lensing data.
- Analyses of the power spectrum of luminous red galaxies (Tegmark et al. 2006; Reid et al. 2010), which can be used to constrain cosmological parameters. In tests with mock galaxy catalogues, Reid et al. (2010) find that a fraction f_{BNC} of 0.2-0.4 results in an angle-averaged LRG power spectrum that is damped by 2 – 4% on scales of $k \sim 0.1 h \text{Mpc}^{-1}$, and the effect is larger at larger k . However, when analyzing the observed power spectrum with these mock catalogues, the effect of f_{BNC} on the recovered cosmological parameters is relatively small.
- Measurements of the radial number density distribution of satellite galaxies, $n_{\text{sat}}(r|M)$, in haloes of mass M . Sev-

eral studies that have measured $n_{\text{sat}}(r|M)$ using groups and clusters have assumed that the halo centre coincides with the location of the BHG (e.g., Carlberg, Yee & Ellingson 1997; Collister & Lahav 2005; Hansen et al. 2005; Yang et al. 2005b). If, instead, the BHG is a satellite galaxy, this will result in an underestimate of the concentration of $n_{\text{sat}}(r)$. Hence, a non-zero $f_{\text{BNC}}(M)$ may cast doubt on the claim, made by several of these studies, that satellite galaxies are less centrally concentrated than the dark matter. On the other hand, Lin, Mohr & Stanford (2004) used the centre of the X-ray emission as the centre of the dark matter halo, rather than the location of the BHG, and came to a similar conclusion.

- Comparisons of the properties of central and satellite galaxies. A number of recent studies have used galaxy group catalogues to split the galaxy population into centrals and satellites, and to compare their properties (e.g., Weinmann et al. 2006, 2009; Skibba et al. 2007; van den Bosch et al. 2008; Pasquali et al. 2009, 2010; Hansen et al. 2009; Kimm et al. 2009; Skibba 2009; Guo et al. 2009). Since all of these studies have assumed the brightest group galaxy to be the central galaxy, they are likely to have underestimated the true differences (i.e., a non-zero f_{BNC} blurs the actual differences between centrals and satellites).

ACKNOWLEDGEMENTS

We thank Darren Croton, for making the results from his semi-analytical model available to us in electronic format, and Eric Bell, Kris Blindert, Romeel Davé, Xi Kang, Tod Lauer, Alexie Leauthaud, Pierluigi Monaco, Beth Reid, Maria Pereira, Simone Weinmann, and Ann Zabludoff for valuable discussions about our results and their implications. Some of the calculations were carried out on the PIA cluster of the Max-Planck-Institute für Astronomie at the Rechenzentrum Garching.

REFERENCES

- Adelman-McCarthy J. K. et al., 2006, *ApJS*, 162, 38
Aubert D., Pichon C., Colombi S., 2004, *MNRAS*, 352, 376
Bailin J., Power C., Norberg P., Zaritsky D., Gibson B. K., 2008, *MNRAS*, 390, 1133
Baldry I. K., Balogh M. L., Bower R. G., Glazebrook K., Nichol R. C., Bamford S. P., Budavari T., 2006, *MNRAS*, 373, 469
Beers T. C., Geller M. J., 1983, *ApJ*, 274, 491
Beers T. C., Flynn K., Gebhardt K., 1990, *AJ*, 100, 32
Bell E. F., McIntosh D. H., Katz N., Weinberg M. D., 2003, *ApJS*, 149, 289
Berlind A. A. et al., 2006, *ApJS*, 167, 1
Bernstein J. P., Bhavsar S. P., 2001, *MNRAS*, 322, 625
Bildfell C., Hoekstra H., Babul A., Mahdavi A., 2008, *MNRAS*, 389, 1637
Binney J. J., Tremaine S. D., 1987, *Galactic Dynamics* (Princeton: Princeton Univ. Press)
Bird C. M., 1994, *AJ*, 107, 1637
Blanton, M. R. et al., 2003, *ApJ*, 592, 819
Blanton M. R. et al., 2005, *AJ*, 129, 2562
Blanton M. R., Roweis S., 2007, *AJ*, 133, 734
Boylan-Kolchin M., Ma C.-P., Quataert E., 2008, *MNRAS*, 383, 93
Cacciato M., van den Bosch F. C., More S., Li R., Mo H. J., Yang X., 2009, *MNRAS*, 394, 929 (C09)
Carlberg R. G., Yee H. K. C., Ellingson E., 1997, *ApJ*, 478, 462
Cohn J. D., Kochanek C. S., McLeod B. A., Keeton C. R., 2001, *ApJ*, 554, 1216
Colless M., et al., 2001, *MNRAS*, 328, 1039
Collister A. A., Lahav O., 2005, *MNRAS*, 361, 415
Conroy C., Wechsler R. H., Kravtsov A. V., 2006, *ApJ*, 647, 201
Conroy C., Wechsler R. H., Kravtsov A. V., 2007, *ApJ*, 668, 826
Conroy C., Ho S., White M., 2007, *MNRAS*, 379, 1491
Cooray A., 2005, *MNRAS*, 363, 337
Cooray A., 2006, *MNRAS*, 365, 842
Corless V. L., King L. J., 2009, *MNRAS*, 396, 315
Coziol R., Andernach H., Caretta C. A., Alamo-Martinez K. A., Tago E., 2009, *AJ*, 137, 4795
Croton D.J., et al., 2006, *MNRAS*, 365, 11
de Vaucouleurs G., de Vaucouleurs A., Corwin H. G., Buta R. J., Paturel G., Fouque P., 1991, *Third Reference Catalogue of Bright Galaxies* (Heidelberg: Springer)
Font A. S., et al., 2008, *MNRAS*, 389, 1619
Giocoli C., Tormen G., Sheth R. K., van den Bosch F. C., 2010, *MNRAS*, 404, 502
Guo Y., et al. 2009, *MNRAS*, 398, 1129
Guo Q., White S. D. M., Li C., Boylan-Kolchin M., 2010, *MNRAS*, 404, 1111
Hansen S. M., McKay T. A., Wechsler R. H., Annis J., Sheldon E. S., Kimball A., 2005, *ApJ*, 633, 122
Hansen S. M., Sheldon E. S., Wechsler R. H., Koester B. P., 2009, *ApJ*, 699, 1333
Hernquist L., 1990, *ApJ*, 356, 359
Hwang H. S., Lee M. G., 2008, *ApJ*, 676, 218
Johnston D. E., et al., 2007, preprint (arXiv:0709.1159)
Kang X., van den Bosch F.C., 2008, *ApJ*, 676, L101
Kimm T., et al., 2009, *MNRAS*, 394, 1131
Kochanek C.S., 1995, *ApJ*, 445, 559
Koester B. P., et al., 2007, *ApJ*, 660, 239
Koopmans L. V. E., Treu T., 2003, *ApJ*, 583, 606
Li C., Jing Y. P., Kauffmann G., Börner G., Kang X., Wang L., 2007, *MNRAS*, 376, 984
Lin Y.-T., Mohr J. J., Stanford S. A., 2004, *ApJ*, 610, 745
Lin Y.-T., Mohr J. J., 2004, *ApJ*, 617, 879
Lo Faro B., Monaco P., Vanzella E., Fontanot F., Silva L., Cristiani S., 2009, *MNRAS*, 399, 827L
Macciò A. V., Dutton A. A., van den Bosch F. C., Moore B., Potter D., Stadel J., 2007, *MNRAS*, 378, 55
Malumuth E. M., Kriss G. A., Van Dyke Dixon W., Ferguson H. C., Ritchie C., 1992, *AJ*, 104, 495
Mandelbaum R., Seljak U., Kauffmann G., Hirata C. M., Brinkmann J., 2006, *MNRAS*, 368, 715
McKay T. A. et al., 2002, *ApJ*, 571, L85
Monaco P., Murante G., Borgani S., Fontanot F., 2006, *ApJ*, 652, 89
Monaco P., Fontanot F., Taffoni G., 2007, *MNRAS*, 375, 1189
More S., van den Bosch F. C., Cacciato M., Mo H. J., Yang X., Li R., 2009, *MNRAS*, 392, 801
Moster B. P., Somerville R. S., Maulbetsch C., van den Bosch F. C., Maccio A. V., Naab T., Oser L., 2010, *ApJ*, 710, 903
Navarro J. F., Frenk C. S., White S. D. M., 1997, *ApJ*, 490, 493
Oegerle W. R., Hill J. M., 2001, *AJ*, 122, 2858
Pasquali A., van den Bosch F.C., Mo H.J., Yang X., Somerville R.S., 2009, *MNRAS*, 394, 38
Pasquali A., Gallazzi A., Fontanot F., van den Bosch F.C., De Lucia G., Mo H.J., Yang X., 2010, *MNRAS*, 407, 937
Postman M., Lauer T. R., 1995, *ApJ*, 440, 28
Reid B. A., et al., 2010, *MNRAS*, 404, 60
Richard J., et al., 2010, *MNRAS*, 404, 325
Rusin D., et al., 2003, *ApJ*, 587, 143
Sanderson A. J. R., Edge A. C., Smith G. P., 2009, *MNRAS*, 398, 1698
Saunders W., et al., 2000, *MNRAS*, 317, 55

- Schlegel D. J., Finkbeiner D. P., Davis M., 1998, *ApJ*, 500, 525
- Scoccimarro R., Sheth R. K., Hui L., Jain B., 2001, *ApJ*, 546, 20
- Shankar F., Lapi A., Salucci P., De Zotti G., Danese L., 2006, *ApJ*, 643, 14
- Sheldon E. S., et al., 2009a, *ApJ*, 703, 2217
- Sheldon E. S., et al., 2009b, *ApJ*, 703, 2232
- Sheth R. K., Mo H. J., Tormen G., 2001, *MNRAS*, 323, 1
- Sheth R. K., Hui L., Diaferio A., Scoccimarro R., 2001, *MNRAS*, 325, 1288
- Skibba R. A., Sheth R. K., Connolly A. J., Scranton R., 2006, *MNRAS*, 369, 68
- Skibba R. A., Sheth R. K., Martino M. C., 2007, *MNRAS*, 382, 1940
- Skibba R. A., Sheth R. K., 2009, *MNRAS*, 392, 1080
- Skibba R. A., 2009, *MNRAS*, 392, 1467
- Skibba R. A., Macciò A. V., 2011, *MNRAS*, in press (arXiv:1103.1641)
- Strauss M. A., et al., 2002, *AJ*, 124, 1810
- Tegmark M. et al., 2006, *Phys. Rev. D*, 74, 123507
- Tinker J. L., Conroy C., Norberg P., Patiri S. G., Weinberg D. H., Warren M. S., 2008, *ApJ*, 686, 53
- Vale A., Ostriker J.P., 2004, *MNRAS*, 353, 189
- van den Bergh S., 1999, *A&AR*, 9, 273
- van den Bosch F. C., Norberg P., Mo H. J., Yang X., 2004, *MNRAS*, 352, 1302
- van den Bosch F. C., Weinmann S. M., Yang X., Mo H. J., Li C., Jing Y. P., 2005, *MNRAS*, 361, 1203 (vdB05)
- van den Bosch F. C., Yang X., Mo H. J., Weinmann S. M., Macciò A. V., More S., Cacciato M., Skibba R., Kang X., 2007, *MNRAS*, 376, 841
- van den Bosch F. C., Aquino D., Yang X., Mo H. J., Pasquali A., McIntosh D. H., Weinmann S. M., Kang X., 2008, *MNRAS*, 387, 79
- Vitvitska M., Klypin A. A., Kravtsov A. V., Wechsler R. H., Primack J. R., Bullock J. S., 2002, *ApJ*, 581, 799
- von der Linden A., Best P. N., Kauffmann G., White S. D. M., 2007, *MNRAS*, 379, 867
- Wang Y., Yang X., Mo H. J., van den Bosch F. C., 2007, *ApJ*, 664, 608
- Wang Y., Yang X., Mo H. J., Li C., van den Bosch F. C., Fan Z., Chen X., 2008, *MNRAS*, 385, 1511
- Weinmann S. M., van den Bosch F. C., Yang X., Mo H. J., 2006, *MNRAS*, 366, 2
- Weinmann S. M., Kauffmann G., van den Bosch F. C., Pasquali A., McIntosh D. H., Mo H.J., Yang X., Guo Y., 2009, *MNRAS*, 394, 1213
- Wetzel A. R., White M., 2010, *MNRAS*, 403, 1072
- White M., Zheng Z., Brown M. J. I., Dey A., Jannuzi B. T., 2007, *ApJ*, 655, L69
- White M., Cohn J. D., Smit R., 2010, *MNRAS*, 408, 1818
- Yang X., Mo H. J., van den Bosch F. C., 2003, *MNRAS*, 339, 1057
- Yang X., Mo H. J., Jing Y. P., van den Bosch F. C., Chu Y., 2004, *MNRAS*, 350, 1153
- Yang X., Mo H. J., van den Bosch F. C., Jing Y. P., 2005a, *MNRAS*, 356, 1293
- Yang X., Mo H. J., van den Bosch F. C., Weinmann S. M., Li C., Jing Y. P., 2005b, *MNRAS*, 362, 711
- Yang X., Mo H.J., van den Bosch F.C., Jing Y.P., Weinmann S.M., Meneghetti M., 2006, *MNRAS*, 373, 1159
- Yang X., Mo H. J., van den Bosch F. C., Pasquali A., Li C., Barden M., 2007, *ApJ*, 671, 153 (Y07)
- Yang X., Mo H. J., van den Bosch F. C., 2008, *ApJ*, 676, 248
- Yang X., Mo H. J., van den Bosch F. C., 2009a, *ApJ*, 695, 900
- Yang X., Mo H. J., van den Bosch F. C., 2009b, *ApJ*, 693, 830
- York D. G. et al., 2000, *AJ*, 120, 1579
- Yoshikawa K., Jing Y. P., Börner G., 2003, *ApJ*, 590, 654
- Zabludoff A. I., Mulchaey J. S., 1998, *ApJ*, 496, 39
- Zaritsky D., Smith R., Frenk C. S., White S. D. M., 1993, *ApJ*, 405, 464
- Zehavi I. et al., 2002, *ApJ*, 571, 172
- Zehavi I. et al., 2005, *ApJ*, 630, 1
- Zheng Z. et al., 2005, *ApJ*, 633, 791